

Unveiling δ Scuti and γ Doradus Hybrid Pulsation of HD 53166 and HD 53349 Plus Rich Frequencies in HD 52788 – Catalogs of 70552 δ Sct and 8080 γ Dor^{*}

Ai-Ying Zhou^{*}

^aNational Astronomy Observatories, Chinese Academy of Sciences, A20 Datun Road, Chaoyang District, Beijing, 100101, P.R. China

Abstract

We present discoveries of the hybrid δ Scuti and γ Doradus types stellar pulsational variability of two stars, HD 53166 and HD 53349, which were previously used as comparison in the differential photometry of a known δ Scuti star HD 52788. More surprisingly, HD 52788 exhibits 126 pulsation frequencies in a small domain in $4\text{--}12\text{ d}^{-1}$ based on 24 sectors light curves of *TESS*. We compared the three stars with up-to-date class members collected from existing catalogs in multiple Hertzsprung-Russell diagrams for checking group property. Two comprehensive catalogs of 70552 δ Sct and 8080 γ Dor stars have been cross-identified with the *TESS* Input Catalog (TIC) and *Gaia* DR3. The catalogs include multiple stellar parameters extracted from both *Gaia* DR3 and TIC v8.2. The rich pulsation contents turn HD 52788 into a rare distinctive object in its class for testing current stellar evolution and pulsation models.

Keywords: stars: oscillation (pulsation), stars: variables: δ Scuti, γ Doradus, techniques: photometric, stars: individual: HD 52788, HD 53166, HD 53349

1. Introduction

The δ Scuti and γ Doradus stars are both pulsating variables that are situated on and near the region of the A and F-type main sequence, inside the lower part of classical Cepheid instability strip (Handler, 2009b; Rodríguez and Breger, 2001; Breger, 2000).

δ Scuti stars (DSCT) are short-period ($\lesssim 0.3$ day) pulsators situated inside the lower part of the classical Cepheid instability strip on and near the main sequence (MS) in the Hertzsprung–Russell diagram, with spectral types ranging from about A2 to F6 for luminosity classes III (giants), IV (subgiants), and V (dwarfs, main sequence stars) (Qian et al., 2018; Szabados, 2014; Gray and Corbally, 2009). They pulsate in radial as well as non-radial acoustic modes excited mainly in the κ mechanism (Breger, 2000; Xiong et al., 2016). The majority of δ Sct stars are multiple mode pulsators. Most of the δ Sct stars belong to the Population I stars that cover a mass range from about 1.5 to 2.3 M_{\odot} (Murphy et al., 2019).

γ Doradus-type variables (GDOR) are a relatively new and small young group of pulsators found over-

lap or just beyond the lower red (cool) edge of the δ Scuti instability strip. This class of variable stars is first characterized in late 1990s (Krisciunas and Handler, 1995; Kaye et al., 1999; Handler, 1999), while γ Doradus itself as the prototype of its class was first revealed to be variable by Cousins and Warren (1963). These stars display longer periods and low-amplitude variability that was confirmed to be caused or characterized by high-order (n), low-degree (ℓ), non-radial, photospheric gravity-type oscillations (g -mode pulsations, Balona et al. 1994; Kaye et al. 1999) rather than the p -mode pulsations of most δ Scuti variables (Krisciunas, 1993; Krisciunas and Handler, 1995; Krisciunas, 1998; Kaye et al., 1999; Handler, 1999). Their multiple periods spaced from several tenths of a day to slightly in excess of one day and pulsational amplitudes usually do not exceed 0.1 mag. Most GDOR stars are typically early F or late A type main sequence stars with ages of ~ 150 Myr. There are hundreds of bona fide GDOR members and a few thousand candidates by far (Henry et al., 2022; Balona and Ozuyar, 2020; Balona, 2022a).

In recent years, a number of stars have been found that exhibit both δ Scuti and γ Doradus type pulsations, such as those discovered in ground observations (Henry and Fekel, 2005; Handler, 2009a; Grigahcène et al., 2010; Hareter et al., 2011; Handler, 2012; Zhang et al.,

^{*}This research is dedicated to my wife Jingyun Zhang who has been supporting my works all the time.

^{*}To appear in New Astronomy, Volume 105, January 2024

Email address: aiying@nao.cas.cn (Ai-Ying Zhou)

2012; Koen et al., 2017) as well as from space missions (Balona et al., 2015; Antoci et al., 2019; Zhang et al., 2020; Balona and Ozuyar, 2020) and even hybrid pulsators in binary systems (Zhang et al., 2019; Ma et al., 2022). Hybrid pulsators, generally speaking, are pulsating stars that show two different types of oscillation features or classified with multiple identities (Zhou, 2015). Particularly in this paper, it refers to the stars that show both γ Doradus type g modes and δ Scuti type p modes. The major observational problem involved in a hybrid pulsator that needs to be solved before arriving at a unique seismic model is more severe than single oscillating type stars – a sufficiently large number of pulsation modes must be detected and identified in both DSCT and GDOR pulsation frequency domains (Handler, 2009c).

On the side of oscillation theory, the low-frequency g modes in γ Dor stars are excited by convective flux modulation (Guzik et al., 2000), but it is not known whether a single excitation mechanism might be responsible for both the p and g modes in hybrid stars (Balona et al., 2015). A recent theoretic study shows that oscillations of δ Scuti and γ Doradus stars are both due to the combination of κ mechanism and the coupling between convection and oscillations, and they belong to the same class of variables at the low-luminosity part of the Cepheid instability strip. Within the δ Sct- γ Dor instability strip, most of the pulsating variables are very likely hybrids that are excited in both p and g modes (Xiong et al., 2016).

The γ Dor, δ Sct, especially those with rich spectrum of pulsation frequencies and the hybrid δ Sct/ γ Dor pulsators offer tremendous potential for asteroseismology (Pollard, 2009; Antoci et al., 2019; Aerts, 2021; Henry et al., 2022). Thus the hybrid pulsators are promising targets for asteroseismology and have the potential to advance the theories of both stellar evolution and pulsation. It is widely recognized to be worthy of detection and characterization of new hybrid pulsators, as their asteroseismic studies would provide new insights into the physics of the oscillations (Henry et al., 2022; Grigahcène et al., 2010). Therefore, the detection of hybrid pulsators is astrophysically significant.

Another interesting research related to DSCT and GDOR is the detection of DSCT or GDOR in eclipsing binary systems, such as those recent works by Chapellier and Mathias (2013); Li et al. (2020a); Chen et al. (2022); Southworth and Van Reeth (2022a).

HD 52788 was announced to be a δ Scuti star by Kurtz (1979). Based on a total of 104 hours of differential photometric observations obtained in 1978–1980, both Kurtz (1981) and Zhou (2004) failed to establish

a consistent frequency solution for the pulsational behaviour of the star. The pulsation frequency spectrum of HD 52788 changed yearly with somewhat complex light variability, makes it a special target in its class.

What makes the author initially interested is the cause of the unstable pulsation frequency spectrum of HD 52788. The poor frequency resolution could result from inadequate time series data, intrinsic rapid changing, and data issues using wrong stars as comparison among others. Which is the true source? Potential comparison stars in the target field were often discovered to be new variables, for example, Du et al. (1999); Zhou et al. (2006); Jurcsik et al. (2012). Due to the star in the southern sky, while the interested observers in the northern hemisphere, the question is that could we have a chance to obtain adequate data to derive a unique set of frequencies that represents the light variations of this star. Fortunately, the NASA’s Transiting Exoplanet Survey Satellite (*TESS*, Ricker et al. 2015) data provide us with the best opportunity to check any star’s light variations more precisely. We are delighted with good fortune when checking *TESS* data. We found rich intrinsic pulsation contents of HD 52788 based on the perfect data sets, and serendipitously we reveal that the two comparison stars used in Kurtz’s differential photometry turned out to be pulsating variable stars (see Fig. 1). This fact of using the wrong comparison would have added uncertainties in resolving the target’s pulsation.

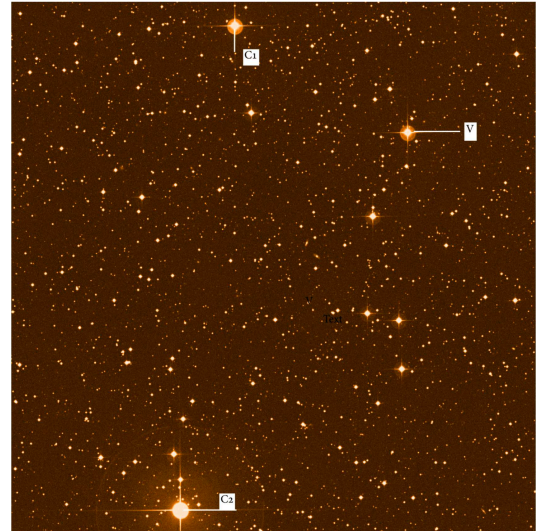


Figure 1: Finder chart of HD 52788 and comparisons used in Kurtz(1979,1981).

This work analyzes the *TESS* light curves of three stars HD 52788 and the two previously used nearby

comparison stars HD 53166 and HD 53349. In Section 2, we describe the *TESS* data and our custom processings, followed by pulsational analyses of the three stars in Section 3. Results and discussions are summarized in the last two sections.

2. *TESS* Data

TESS is an MIT-led NASA mission dedicated to discovering transiting exoplanets orbiting nearby bright stars by an all-sky photometry survey (Ricker et al., 2015). *TESS* spacecraft launched on April 18, 2018 and its regular science operations began on July 25, 2018. *TESS* rotates every ~ 13.7 days per cycle along a unique highly elliptical lunar-resonant orbit around the Earth (about 600 km from Earth). *TESS* is equipped with four identical refractive cameras with a combined field-of-view (FOV) of 24×96 degrees (a segment of sky, known as an observing sector). The lens assembly in each camera has a 10.5 cm diameter entrance pupil (aperture) and a focal ratio $f/1.4$. Each of the four cameras has four 2048×2048 CCD detectors (i.e. total 16 CCDs). Each detector pixel sized 15×15 micron corresponds to 21 arcseconds in the sky. *TESS* collects light in 600–1000 nm centered on the traditional Cousins *I*-band (I_C , central wavelength = 786.5 nm). Please refer to the details to *TESS* Science Data Products Description Document¹ and “Characteristics of the *TESS* space telescope” web page². *TESS* filter basically matches with *Gaia* Red Photometer with bandpass spanning in 630–1050 nm (Gaia Collaboration et al., 2016).

TESS cameras actually expose at a cadence of 2 seconds. That is, the CCDs take images and read them out continuously at 2-second intervals. However, the 2-second frames are used for spacecraft guiding, they were not downloaded to the ground. The images are processed on the spacecraft by the data handling unit (DHU, a Space Micro Image Processing Computer). The DHU stacks 2-second images in groups of 60 or 900 to produce 2-minute cadence images (in cut Target Pixel File, TPF) and 30-minute cadence for general observations. High cadence is needed for the detection of exoplanets, so exposures of planet search targets and other stars of particular interest (cataloged 200,000 primary stars) are obtained every 2 minutes while the Full-Frame

Images (FFIs) of the entire field of view are returned every 30 minutes. Finally, pixels in postage stamps around *TESS* mission target stars will be downloaded at a 2-minute cadence, while FFIs will be downloaded at the 30-minute cadence. These two sets of data will allow general variability studies for the vast majority of stars. The data on spacecraft are transmitted to Earth when the spacecraft reaches orbital perigee every ~ 13.7 days. Each sector of the sky will be observed twice with 27.4 days observing period. So the *TESS* observation is most sensitive to exoplanets with periods of less than 13 days so that at least two transits are used for discovery.

In the meantime, *TESS* high-precision uninterrupted photometry and time resolution (2-minute and 30-minute cadence) are perfect for stellar pulsation and asteroseismology (e.g. the works by Lund et al. 2021; Handberg et al. 2021). Furthermore, *TESS* produces additional pixels in little postage stamps surrounding a few bright asteroseismology targets and downloads at 20-second cadence (1000 stars, e.g. the works by Huber et al. 2022). After *TESS* first two-year prime mission, started in July 2020, *TESS* was revisiting the sky in an extended ongoing mission that records full-frame images at a fast ten-minute cadence. *TESS* provides a golden opportunity for studying short to moderate long periodic variables, in special, δ Sct and γ Dor stars (Antoci et al., 2019), RR Lyr stars and so on.

We first checked the *TESS* archive at the MAST Portal (Mikulski Archive for Space Telescopes³) for available data of the interested target star HD 52788 (=V383 Carinae =TIC 279361762 =ASASSN-V J065904.08-583054.1, $\alpha_{2000}=06:59:04$, $\delta_{2000}=-58:30:53$ [104.7667° , -58.5147°], $V=8^m.40$) and the two comparison stars used in literature C1=HD 53166 (=TIC 279431011, $V=8^m.1$) and C2=HD 53349 (=TIC 279476396, $V=6^m.01$). We downloaded the NASA’s Science Processing Operations Centre (SPOC) generated files, including both the extracted light curves (*.s_lc.fits) and Target Pixel files (*.s_tp.fits). The light curve files *.s_lc.fits will be read directly with *ASTROPY* and *LIGHTKURVE* packages (The Astropy Collaboration et al., 2018a,b) in a Python script following the *TESS* Archive Manual⁴. The *TESS* data information for these three stars is listed in Table 1.

¹<https://archive.stsci.edu/missions-and-data/tess/>; https://archive.stsci.edu/files/live/sites/mast/files/home/missions-and-data/active-missions/tess/_documents/EXP-TESS-ARC-ICD-TM-0014-Rev-F.pdf

²<https://tess.mit.edu/science/> or <https://heasarc.gsfc.nasa.gov/docs/tess/the-tess-space-telescope.html>

³<https://mast.stsci.edu/portal/Mashup/Clients/Mast/Portal.html>; or <https://archive.stsci.edu/tess/>

⁴The Beginner Tutorial Notebooks: <https://outerspace.stsci.edu/display/TESS/TESS+Archive+Manual>; https://github.com/spacetelescope/notebooks/blob/master/notebooks/MAST/TESS/beginner_how_to_use_lc/beginner_how_to_use_lc.ipynb

2.1. SAP and PDCSAP

There are two kinds of SPOC-extracted light curves: one is Simple Aperture Photometry flux (SAP), which is the flux after summing the calibrated pixels within the *TESS* optimal photometric aperture, and the other is Pre-search Data Conditioned Simple Aperture Photometry (PDCSAP), it is the SAP flux from which long-term trends have been removed using so-called Co-trending Basis Vectors and nominally corrected for instrumental variations and excessive scattered light removed. Figure 2 shows two cases of the two kinds of light curves. PDCSAP flux is usually cleaner data than the SAP flux and will have fewer systematic trends. Thus PDCSAP flux is widely used for final analysis without further processing (e.g. Dumusque et al. 2019; Astudillo-Defru et al. 2020; Demory et al. 2020; Battley et al. 2021). However, the PDCSAP flux might suffer from loss or wrong-deletion of long-term and transient burst variability intrinsic to stars, for instance, as that pointed out by Hill et al. 2022; Littlefield et al. 2021. With these concerns, SAP flux is used by some authors (e.g. von Essen et al. 2020; Steindl et al. 2021; Hon et al. 2021; Prša et al. 2022; Southworth and Van Reeth 2022b) accompanied with additional custom processing such as detrendings depending on science goals.

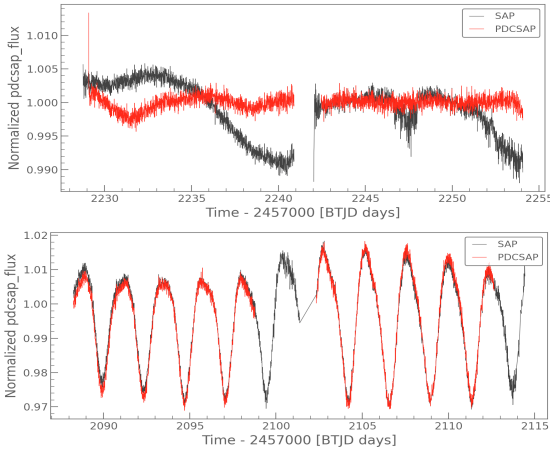


Figure 2: Comparison between TESS SAP and PDCSAP fluxes of two variable stars. Up: this case PDCSAP will be used; down: SAP can be used.

We then checked the two comparison stars in General Catalog of Variable Stars (GCVS database, Version 2022 Jun. and 5.1, Samus et al. 2017)⁵ and Revised Version of the New Catalogue of Suspected Variable Stars (NSV Release 2, 1982, 1998, Kazarovets et al. 2022)⁶,

⁵online URL: <http://www.sai.msu.su/gcvs/cgi-bin/search.htm#cat>

⁶<https://heasarc.gsfc.nasa.gov/W3Browse/all/gcvnsvars.html>

and found that C2=HD 53349 =HR 2661 =NSV 3349 is a dwarf (DM, spectral type F0V) and a new suspected variable star but without further information. We further looked for *TESS* Input Catalog (TIC) v8.2 and CTL v8.01 catalog (Stassun et al., 2018, 2019; Paegert et al., 2021), and adopted the basic astronomical parameters in Table 2.

Table 1: *TESS* observations (at two-minute cadence) of HD 52788, HD 53166 and HD 53349.

Star Identifiers	V	Sp. Type
V =HD 52788 = TIC 279361762	8 ^m 37	Fm_dD
C1=HD 53166 = TIC 279431011	8 ^m 1	A1V
C2=HD 53349 = TIC 279476396	6 ^m 0	A8III or F0V
Orbits; Sector (Camera,CCD)	11–25, 61–85;2–10,12,13,27–39 (4,4),(4,1),(4,3),(4,2) S0036 started on 2021 Mar 1	
Time span	BJD 2458354.107–2459389.716 (2018 Aug 22 23:50–2021 May 26 02:43UT,1035.6 days)	
Data length	24 sectors * 13.7 days * 2 = 657.599 days	
Frequency resolution	0.0009656 d ⁻¹	
Number of data points analyzed	419,915 (outliers and unusual data points excluded)	
Total number of data	422,046	

2.2. Custom Data Processing

In the current work, we first did graphic screenings on each sector’s light curves for choosing SAP or PDCSAP flux. A close visual inspection of both light curves plotted up and down and overlapping helped the author compare which one is better for pulsation detection. If the SAP flux looks no evident difference with PDCSAP flux, then use SAP flux. If the PDCSAP flux data lost too many points while the SAP flux data are flat, then we choose SAP flux, otherwise, especially in the case of severe systematic trends showing slope and steep brightness, PDCSAP flux is chosen. Figure 2 shows two examples. In any SAP or PDCSAP flux, those data points flagged as “bad quality” were removed.

During a course of surveying a large amount of *TESS* light curves the author found that both PDCSAP and SAP fluxes could be sometimes suffered from a systematic shift in brightness between the two orbits of a *TESS* sector, which would result in abnormal discontinuity and artificial displacement of the two orbits’ light curves. This is quite frequently occurred in HLP-QLP (uncorrected SAP) light curves

for long-period variables, for instance, Mira variables TIC 329891910, TIC 457021714, and TIC 359401246 on sector 38. Displacements of a segment light curve also occurred within individual orbits, e.g. RRLyr star TIC 127088233 on sector 38 and so on. Thus, a custom processing of correction to the displacement is applied whenever needed. With the above criteria, these final used fluxes of PDCSAP and SAP mixture are ensured the *TESS* best estimate of the intrinsic variability of a target. Any remained low-frequency instrumental systematics would be either not removed or introduced by the *TESS* reduction pipeline (Cunha et al., 2019).

Table 2: Astronomical Parameters of HD 52788, HD 53166 and HD 53349.

Para.	V=HD 52788	C1=HD 53166	C2=HD 53349
<i>B</i>	8.788±0.028	8.27±0.027	6.283±0.023
<i>V</i>	8.39±0.03	8.15±0.03	6.01±0.03
<i>J</i>	7.683±0.024	8.07±0.026	5.422±0.018
<i>H</i>	7.521±0.027	8.045±0.024	5.296±0.023
<i>K</i>	7.473±0.029	8.006±0.023	5.245±0.016
Tmag	8.0396	8.17	5.722
Sp. type	Fm_dD	A1V	A8III
T_{eff}	6838±134.87	9562±186.18	7118.48±111.54
log <i>g</i>	3.319±0.092	4.21±0.06	4.039±0.079
<i>R/R</i> _⊙	4.412±0.216	2.026±0.053	1.988±0.069
<i>M/M</i> _⊙	1.48±0.25	2.43±0.32	1.59±0.25
<i>L/L</i> _⊙	38.35	30.93	9.15
<i>M_V</i>	0.987	1.304	2.335
<i>D</i> (pc)	302.42	234.1	54.3

Last, we proceed to process the *TESS* data. The fluxes (SAP_Flux and PDCSAP_Flux) corresponding magnitudes (SAP_mag and PDCSAP_mag) are calculated using the formula $\text{mag} = -2.5 \log(\text{flux}) + 20.4436$. The magnitude zero point was selected for a resulting magnitude matching with Tmag of TIC v8.2. By arbitrarily selecting a star, TIC 41196013 (Tmag=11^m.4745) which was observed in *TESS* sector 41 and confirmed as a non-variable in a time scale of days for calibrating the magnitude zero point. We found 20.4436 and 20.2531 mag for converting SAP and PDCSAP fluxes into magnitudes, respectively. In case of two successive orbits observations (each ~13.7 days) having different mean values, a unique zero mean was applied for Fourier analysis.

Such flattening to a uniform level by subtracting individual means of each part was also applied to the uneven cases from sector to sector. Therefore light curves be-

tween two orbits and among sectors are always lined up before doing Fourier analysis. This adjustment of magnitude zero points ensures the elimination of externally-entailed additional noise in the low-frequency domain. Concerning no atmospheric effect on the *TESS* photometry, it is not necessary to establish differential magnitude as in traditional ground photometry. Thus the above-calculated magnitudes were used in our analyses. This way also allows us to diagnose each star without effects brought in by comparison stars.

3. Frequency analysis

We analyze pulsation contents by resolving light curves into a sum of multiple sine or cosine waveforms with different frequencies, amplitudes, and phases through classical Fourier transform. Fourier analysis was carried out by using PERIOD04 (Lenz and Breger, 2005). It is known that noise in low-frequency domain, aliasing, and false peaks caused externally are three key issues which should be noticed in Fourier analysis. Caution was taken in picking up a frequency when strong low-frequency instrumental noise is present even though our custom processing of *TESS* SAP and PDCSAP light curves data has exerted in minimization of external sources.

It is well known that stellar activities may not be periodic, and even irregular. Periodic signals including pulsation are not strictly sinusoidal. Deviations of multiple sines to light curves need careful evaluation. Therefore, when the residuals of least-squares fitting of multiple frequencies to light curves improve insignificantly, we have to stop prewhitening. Moreover, we pick up frequencies over a signal-to-noise (SNR) level of 4.3 following Breger et al. (1993). We recalculated residuals and SNR with the remained significant frequencies.

Aliasing in Fourier spectrum is resulted from discrete data sampling. Ground astronomy has various sampling intervals and daytime gaps without data. Uninterrupted space observations never mean no interruption in observations, they are still true discrete sampling in time-space. *TESS* exposed every two seconds, HDU stacked images into groups of 2-minute cadence and 30-minute cadence for different science goals. Data-downloading periods together with orbits and sectors switch, these are actual *TESS* data sampling intervals. Aliasing, as a data acquisition effect caused by sampling intervals is not yet completely eliminated in space-based data.

Here we explored the *TESS* data aliasing. First, similar to Shporer et al. (2019), the data points showing severe residual uncorrected systematics in the fits are removed in the joint analysis presented in this paper. We

know that single-site ground-based photometry was affected by daily aliases, which occur when observations are not made during the day and the next night's observations begin almost 24 hours later. Under Nyquist sampling theorem, frequencies less than half the sampling rate will not alias: $f_{\max} = 1/(2\Delta t)$. *TESS* observations' sampling intervals are 2 and 30 minutes, that means the maximum possible frequencies (i.e. the Nyquist frequency) should be less than 360 and 24 d^{-1} , respectively. However, besides the regular sampling intervals, there are additional time gaps in *TESS* data sets between two consecutive orbits in a sector as well as between two successive sectors. The gaps in the middle of each sector's time series are due to the data downlink separating the two physical orbits within each *TESS* sector.

The current available *TESS* data for the three targets cover 24 sectors across the 2nd to 39th sectors (see Table 1). This set of data spanned 1035.61 days, starting on BJD 2458354.10718 to 2459389.71673 (i.e. between 2018.08.23 14:33 and 2021.06.24 05:12). Besides regular orbits and sectors switch intervals – actually they are not fixed and they depend on the pipeline reduction of PDCSAP (roughly in 1.0–4.0 days in current case⁷), there are no data available in sector 11 and sectors 14 through 26 over the entire 2nd to 39th sector period. As a composite effect, the spectral window reflects the real aliasing structure. Figure 3 shows the spectral window, which is much sharp. Two stronger aliases are marginal in the zoomed graph at $a_1=0.001302$ and $a_2=0.004314 \text{ d}^{-1}$. Nyquist sampling theorem indicates that a frequency peak will be accompanied by the combination side peaks at $f \pm a_1$ and $f \pm a_2$. Due to the aliases are actually weak, each side peak will less contaminate intrinsic frequencies and will be not further aliased to harmonic spaces of either a_1 or a_2 in our case. Under the above scheme, the final derived periods have ejected all possible aliases.

In addition, the frequency resolution of the time-series data is an important consideration when identifying closely spaced frequencies in periodograms. The frequency resolution of a Fourier transform denotes the smallest frequency difference that can be distinguished. A higher frequency resolution allows for better discrimination between closely spaced frequencies. The frequency resolution is determined by the length of the time series and the sampling rate by the following formula: $\Delta f = f_s/N$ where f_s is the sampling rate and N is the number of data points used in the FFT. It follows that better frequency resolution can be achieved using

a longer data sequence. Assuming 2-minute cadences sampling rate with total 419915 data points analyzed, the resulting frequency resolution is $\Delta f=0.001715 \text{ d}^{-1}$.

Alternatively, the frequency resolution is restricted by the total time base length (T) of a dataset following the traditional Rayleigh criterion and is theoretically defined by $\Delta f = 1/T$, which would result $\Delta f=0.0009656 \text{ d}^{-1}$ if we used the time span $T=1035.61$ days across over sectors 2 to 39. In current case, the effective time coverage with data is 24 sectors having 48 orbits, the actual time duration equals to $T_r \sim 13.7*48 = 657.6$ days, that is 63.49% of the above observing time span (refers to Table 1). Thus an alternative effective frequency resolution would take the value of $1/657.6 = 0.00152068 \text{ d}^{-1}$. This value implies a much conservative frequency resolution of about $1.6/T$, a coincidence with the argument of $1.5/T$ as the resolvable frequency spacing (Loumos and Deeming, 1978). However, we learned that Kallinger et al. (2008, 2017) suggest a less conservative criterion of $1/(4T)$ based on Monte-Carlo simulation.

Taking a further comparison with the *Kepler* light curve of the δ Sct star KIC 7106205 which spans a total of 1470 d (4 yr) consisting of 65 308 data points where the frequency resolution was $1/T=0.00068 \text{ d}^{-1}$ (Bowman and Kurtz, 2014), if one used sample frequency divided by the number of data points as frequency resolution (i.e. $\Delta f = f_s/N$), then it would be only 0.0226 d^{-1} assuming the short cadence data. The later value is 33 times of the previous one. In this regard, the above calculated value of $\Delta f = f_s/N = 0.001715 \text{ d}^{-1}$ (roughly equals to $2/T$) for the present 24 *TESS* sectors data was over-estimated. It is a known shortcoming that the *Kepler* short and long cadence data have integration times of 58.5 s and 29.5 min, respectively, not good for detection of short time-scale variations and close frequencies given limited frequency resolution (Southworth et al., 2011; Murphy, 2012). *TESS* has better data coverage within a sector with shorter cadence sampling, the frequency resolution of 24 *TESS* sectors is excellent and it's value should not be over-estimated.

Now with these estimations used in the literature, we can reach a good compromise with a particular emphasis on continuous space photometric data. As the geometric mean is less affected by extreme values than the arithmetic mean, we propose to derive the weighted geometric mean of the three estimations $1/(4T)$, $1.5/T$ and $1/T$ with respective weights of 2, 0.5 and 1 calculated by

$$\Delta f_1 = \sqrt[3.5]{\left(\frac{1}{4T}\right)^2 * \left(\frac{1.5}{T}\right)^{0.5} * \frac{1}{T}} \approx \frac{1}{2.1T} \quad (1)$$

⁷TESS observing dates refer to: <https://heasarc.gsfc.nasa.gov/docs/tess/sector.html>

and then the weighted geometric mean of the two extreme estimations $1/(4T)$ and $1.5/T$ with respective weights of 2 and 1 calculated by

$$\Delta f_2 = \sqrt[3]{\left(\frac{1}{4T}\right)^2 * \frac{1.5}{T}} \approx \frac{1}{2.2T} \quad (2)$$

Last take the arithmetic mean of the two geometric means, we get

$$\Delta f = \frac{\Delta f_1 + \Delta f_2}{2} \approx \frac{1}{2.15T} \quad (3)$$

Assigning double weight to $1/(4T)$ is a deliberate strategy in regard to the high accuracy and perfect time coverage of the 24 *TESS* sectors data. So taking account of large amount of accurate well-sampled space data we are able to confidently adopt a realistic estimation of $\Delta f = 1/(2.15T) = 0.000449 \text{ d}^{-1}$ as the smallest distinguishable frequency difference when resolving two closely spaced pulsation contents for the 24 *TESS* sectors data. Two close significant frequencies with a separation larger than 0.000449 d^{-1} will be taken as two individual frequencies, otherwise one frequency.

Nevertheless, the frequency resolution criterion itself could dramatically over-estimate the real uncertainty in frequencies. Frequency resolution is related to the error in frequencies by the formula

$$\sigma_f = \sqrt{\frac{6}{N}} \frac{1}{\pi T_r} \frac{\sigma(m)}{a} \quad (4)$$

where a is amplitude, N is the number of analyzed data points, $\sigma(m)$ is the root-mean-squares (rms) of a least-squares sinusoidal fit and $T_r \equiv N\Delta t$ is the total time length of the data (see eq.(11) in Montgomery and O'Donoghue, 1999) other than the above observing time span in most cases.

For the Fourier parameters resulted from PERIOD04, which also calculated the analytical uncertainties on each frequency, amplitude, and phase of the best-fitting sinusoids following the formulae derived by both Montgomery and O'Donoghue (1999) and Breger et al. (1999). We have assumed the residuals from the multiple frequencies least-squares fitting to be the root-mean-squares (rms) deviations of observational noise corresponding to the 24 sectors data set, i.e. $\sigma(m) = 0.00273 \text{ mag}$. Learned from Kallinger et al. (2008) who explored the Fourier parameters errors in detail, the above determined errors would not be underestimated.

4. Results

We report in this section our results for each analyzed star in tables of frequency solution and in graphs of light curves, periodograms and prewhitened residuals.

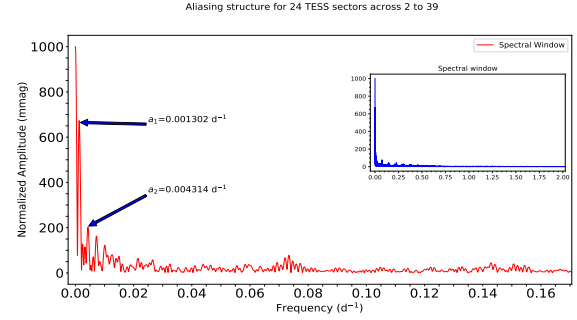


Figure 3: Aliasing structure for the combination data of 24 *TESS* sectors 2–10, 12, 13, 27–39.

4.1. HD 52788 = TIC 279361762

TESS observed HD 52788 in total of 24 sectors across 2 to 39 over 1035 days from 2018 August 22 through 2021 May 26. Light curves are available as sources of *TESS*-SPOC, HLSP-QLP, and HLSP-SPOC. The *TESS*-SPOC 2-minute cadence SAP flux data were used. We see the MIT HLSP-QLP team attempted resolving the data with multiple planets fittings, but no final prospective outcome. The light curves exhibit a much more complex structure visually. With successive prewhitenings and multiple frequencies fittings, the residuals are improved slightly (see Table 3), more frequencies do not satisfactorily account for the complexity of the light curves of HD 52788. With a big number of parameters when simultaneous optimization for frequencies, amplitudes, and phases, non-linear least-squares fitting encountered a divergent issue of 'matrix cannot be inverted', which failed to improve the three parameters of the fitting. So we have to stop prewhitening procedure when reaching the 191st trial frequency. Then we computed noise levels based on both residuals and original data for comparison of significant peaks. Though up to 191 trial frequencies were prewhitened in the procedure, 135 frequencies with significant signal-to-noise ratios over 4.3 were screened out. Then multiple frequencies least-squares fitting using the 135 frequencies was done, and the residuals, noise level and SNR were recalculated. We applied the frequency resolution adopted above of 0.000449 d^{-1} to discriminate close frequencies and finally a total 126 individual significant pulsation frequencies are remained, along with 3 combination terms and 9 significant frequencies under resolving limit. Frequency analysis shows that the residual spectrum even with 135 frequencies pre-whitened is still full of peaks in the range of 5–15 d^{-1} over the calculated significant curve using residuals but below that calculated from original data (see the insert of Fig. 4). Table 4 re-

ports the final results, where the errors for frequency and phase are given in a compact uncertainty notation way. The number in parentheses represents the uncertainty of the measurement and it is expressed as one standard deviation (1σ). Figure 4 displays the light curves on a sector and periodogram based on all 24 sectors data.

Table 3: Residuals of Multi-frequency Least-Squares Fitting with Successive Prewhitenings.

Number of Frequencies	Residuals of Fitting	Improvement Rate
12	0.0042389	—
32	0.0032422	23.5%
79	0.0030626	5.54%
108	0.0030232	1.29%
120	0.0029725	1.68%
158	0.0028472	4.22%
169	0.0028147	1.14%
191	0.0027301	3.01%

4.2. HD 53166

HD 53166 (=TIC 279431011, $V=8^m17$, A1V, RA=07:00:34.60, Dec=−58:23:36.26 J2000.0), its *TESS* light curves are available on sectors 2–13 in both 2-minute cadence (SPOC products) and 30-minute cadence (TASOC, TESS-SPOC, and QLP), and on sectors 27–39 as HLSP-QLP products in cadence of 10-minute. Total 24 sectors. With *TESS* data we reveal the star seems to be a new γ Doradus and δ Scuti hybrid pulsating variable star. Pulsation frequency contents are given in Table 5. Figure 5 shows the light curves on sector 12 and periodograms for the 2-minute cadence data on sectors 2–12 together with the 10-minute cadence data on sectors 27–39, respectively.

4.3. HD 53349

HD 53349 (=HR 2662 = TIC 279476396, $V=6^m0$, A8III, RA=07:01:05.11 Dec=−58:56:23.77) is a high proper motion star. It was listed as NSV 3349 with F0V spectral type in the International Variable Star Index (VSX) of AAVSO but without an identified variability type⁸. Actually, the light variation is hardly visible from any single sector data. Analyses based on both the sector 36th and all available 24 sectors between 1st and 39th consistently lead to multi-periodic pulsational variations with two dominant frequencies at $f_1=1.888139$

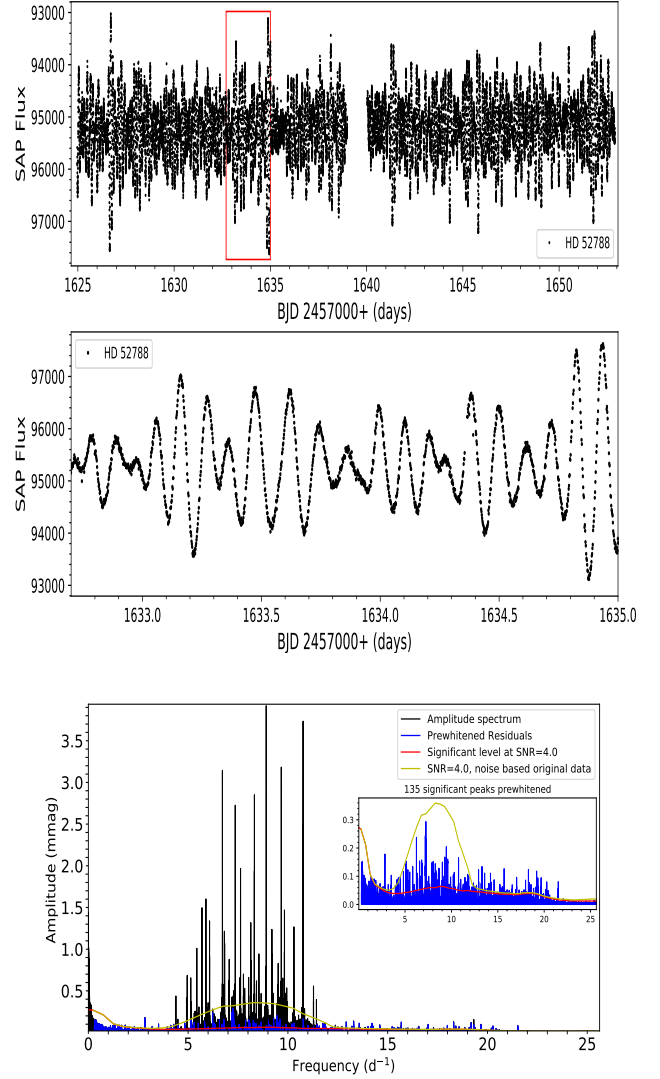


Figure 4: *TESS* light curves of HD 52788=TIC 279361762 (Top: on sector 12; Middle: the red portion zoomed-in) and the amplitude spectrum using all 24 sectors (2–10, 12,13, 27–39).

and $f_2=1.809503\text{ d}^{-1}$. Figure 6 shows the periodograms for the 36th sector and the 24 sectors out of 1–39 at 2-minute cadence, respectively. Frequency solution is reported in Table 6.

5. Discussion and Conclusion

With 24 *TESS* sectors consisting of 48 orbits, each orbit ~ 13.7 -day uninterrupted high-precision photometry we are able to insight the real nature of the light variations of the known δ Sct star HD 52788 (=V383 Car). Surprisingly, we reveal that the two comparison stars HD

⁸<https://www.aavso.org/vsx/index.php?view=search.top>

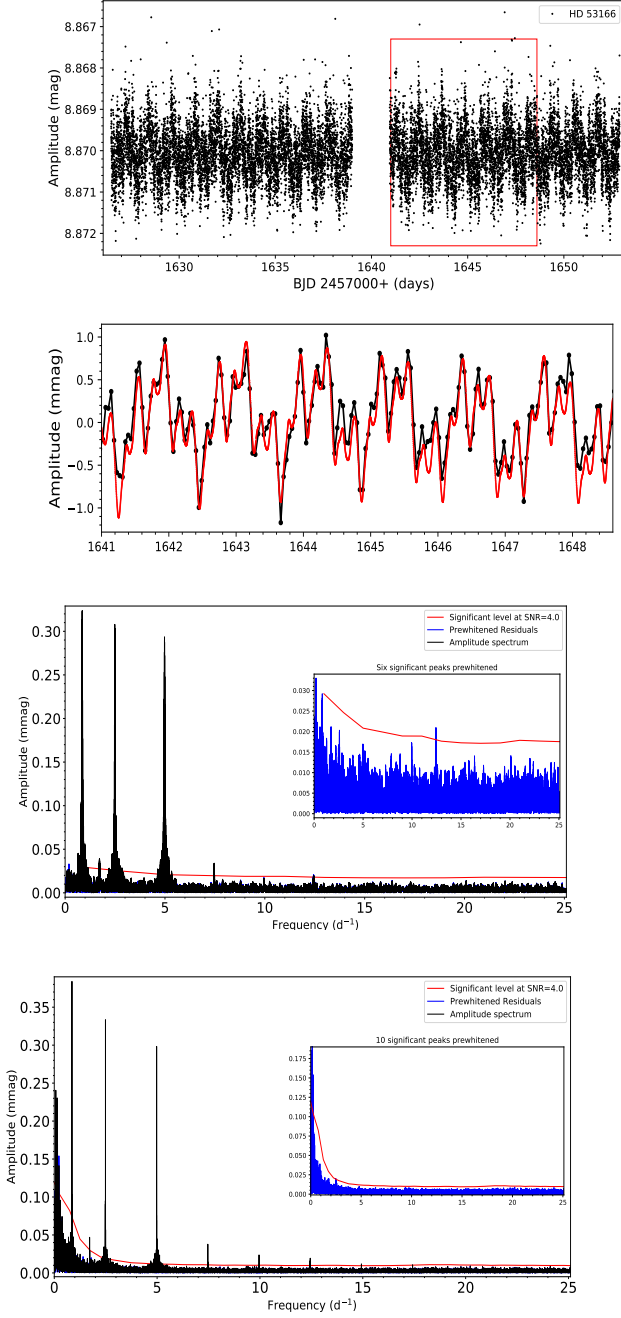


Figure 5: Light curves and amplitude spectrum of HD 53166=TIC 279431011. Top: on sector 12; second panel: the red portion zoomed-in with fitting in red; third panel: 2-minute cadence on sectors 2–12; bottom: 10-minute cadence on sectors 27–39.

53166 and HD 53349 used in the only existing differential photometry of HD 52788 in the literature are now identified to be γ Dor and δ Sct hybrid variable stars. We unveiled the variability types and pulsation contents for the three targets down to an unprecedented precision

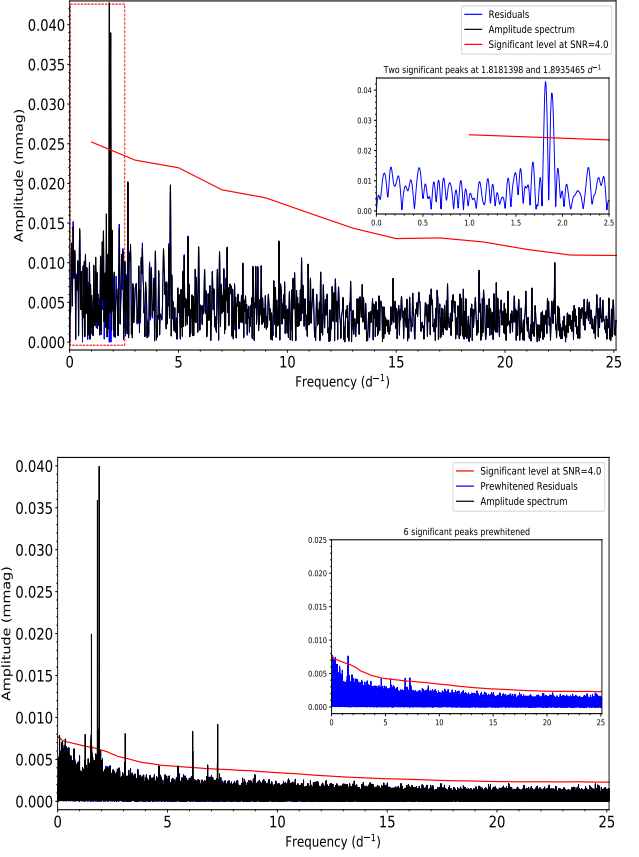


Figure 6: Amplitude spectrum of HD 53349 (=TIC 279476396). Top: sector 36, bottom: 24 sectors.

of pulsational amplitudes 5.7, 16, and 8 μ mag, respectively.

5.1. HD 52788

Compared with previous ground results, the primary frequency $f_0=10.765 \text{ d}^{-1}$ is stable. The two old frequencies around 9.688 and 8.885 are changed and they should be blended mixture of multiple unresolved close frequencies. Surely a few days of the old dataset is too constrained to allow a good frequency resolving power as the present 24 sectors data spanning 1035.6 days with actual data length of 657.599 days which indicate a theoretic frequency resolution of 0.0009656 d^{-1} and an effective frequency resolution of $0.00152068 \text{ d}^{-1}$, respectively. Instead of using these two much conservative thresholds $-1/T$ and $1.6/T$, based on literature data, we derived an empirical frequency resolution of $\Delta f = 1/(2.15T)=0.000449 \text{ d}^{-1}$ as a discriminating cri-

terion for distinguishing closely spaced frequency contents accounting for the large amount of accurate space data. Because the pulsational contents of HD 52788 are mainly in the range of $4\text{--}12\text{ d}^{-1}$, and the three strongest frequencies of both HD 53166 and HD 53349 are lower than 5 d^{-1} , HD 52788 should have not been significantly affected by the two comparison stars involved in the differential photometry in the previous studies. The amplitudes of C2=HD 53349 are so small (smaller than 60 micro-magnitude) that they would not influence in the results of the analysis of the light curves obtained with the old ground-based photometric observations of HD52788. However, in the case of C1=HD 53166, the amplitudes are somewhat larger. HD 53166 could have had some influence on the primary peaks of HD52788 in the previous studies. The pulsation frequency spectrum of HD 52788 over 126 individual frequencies is outstanding and rare among the δ Sct stars. Such a good number of pulsation frequencies deserve a follow-up asteroseismic analysis in a separate work.

In Breger et al. (2005), 75+ frequencies for the famous δ Sct star FG Virginis were resolved using extensive photometric multisite campaign data. Guzik et al. (2022) re-visited FG Vir using *Kepler* K2 and *TESS* data and found around 30 significant frequencies in the K2 data, and more than 100 significant frequencies in the *TESS* data. FG Vir was observed for 52 days in 30-minute cadence photometry by the NASA *Kepler* spacecraft K2 mission in 2016, and for 23 days in 2-minute cadence photometry by the NASA *TESS* spacecraft in 2021. Apparently, *TESS* observations of present targets are much longer than that of FG Vir. Now, with a total of 24 sectors *TESS* data, HD 52788 with 126 frequencies easily overpasses FG Vir, brings itself to the top tier of δ Sct-type stars with rich pulsation contents. This is comparable with the hot white dwarf pulsator PG 1159-035, in which a total of 107 frequencies were identified with 69 days of the *Kepler* satellite K2 mission 59 s cadence data and 25 days of the *TESS* satellite 20 s cadence data by Oliveira da Rosa et al. (2022). One can also compare it with an earlier work based on *CoRoT* timeseries which revealed HD 50844 with hundreds of terms in the frequency range $0\text{--}30\text{ d}^{-1}$ (Poretti et al., 2009; Chen et al., 2016). These authors and Balona (2014) confirmed an initial guess that δ Sct stars have a very rich frequency content. So HD 52788 would not be alone in frequency richness, more pulsators with dense frequencies will appear with further analyses of *Kepler* and *TESS*-like space data. In fact, additional examples have been published, for instance: the binary pulsating subdwarf B star KIC 11558725 with an invisible white dwarf was revealed to have the pulsational con-

tent of more than 160 significant frequencies based on near-continuous 2010-2011 *Kepler* light curves (Telting et al., 2012). Shi et al. (2021a) resolved 200+ pulsation frequencies in an oscillating Algol-type eclipsing binary system HL Dra with 13 *TESS* sectors data (over a timespan of 352 days). Breger et al. (2012) and Breger and Montgomery (2014) revealed 349 statistically significant frequencies of the rapidly rotating δ Sct/ γ hybrid KIC 8054146 using short-cadence *Kepler* data during quarters Q2.3 and Q5 to Q10 which covered a time span of 27 and 557 days, respectively. We can further expect huge discovery opportunities of longer periodic variables provided by *TESS*, *LSST* (Ivezić et al., 2019) and other similar surveys in the near future.

5.2. HD 53166 and HD 53349

HD 53166 is completely a newly discovered variable star, while HD 53349 is collected in VSX and GCVS as NVS 3349 without a variability type. Based on their spectral types, effective temperatures and detected frequencies domain, both stars are now identified to be γ Dor and δ Sct hybrid pulsators. The three strongest frequencies of both stars: HD 53166 at $0.8599, 2.4588, 4.9776\text{ d}^{-1}$; HD 64339 at $1.888139, 1.809503, 1.538036\text{ d}^{-1}$, are well in the γ Dor pulsation domain, together with a couple of frequencies over 6 d^{-1} fitting the δ Sct pulsation. The above identification has followed the recent δ Sct class prototype δ Scuti (=HD 172748) advancement (Daszyńska-Daszkiewicz et al., 2021), γ Dor-type descriptions of Paunzen et al. (2020), γ Dor and δ Sct hybrid demonstrations of Zhang et al. (2020, 2012); Rowe et al. (2006), and the earlier suggestion by Grigahcène et al. (2010), who proposed a division into 'pure' DSCT stars ($f > 5\text{ d}^{-1}$), 'pure' GDOR stars ($f < 5\text{ d}^{-1}$), and hybrid-types exhibiting variability in both frequency regimes.

In respect to the resolved frequencies and variability types, alternative explanation could be that the light variation profile of HD 53166 might be a kind of rotational modulation. f_0 is very probably the rotational frequency. If the theoretic and effective frequency resolution 0.0009656 and 0.00152068 d^{-1} were ignored, f_3 is very closed to f_0 by a difference of 0.003006 d^{-1} , which would be an indication of differential rotation (spots were moving along the stellar surface), together with $f_4 = 2f_0 + 0.003006\text{ d}^{-1}$ being possible harmonics. On the other hand, $f_1, 2f_1, 3f_1, 4f_1, 5f_1, 6f_1$ are very probably binarity cause with f_1 being the orbital frequency (corresponding orbital period of 0.40 d). Thus this star could be a non-pulsating star, but a rotational variable in an eclipsing binary system of probably of the β Lyr type

with the depth of the secondary eclipses much smaller than those in the primary ones (Rodríguez, 2023).

Similarly, the third frequency term f_2 of HD 53349 could be regarded as a rotational frequency, and then $f_4 = 4f_2 - 0.003954$, $f_5 = 2f_2 + 0.00157$. In Fig. 6 there is another peak, nearly significant, close to $3f_2 = 4.61 \text{ d}^{-1}$. An additional γ Dor pulsation peak at $f_7 = 1.2517 \text{ d}^{-1}$ is slightly over significant level. In resolving frequencies, we noted another peak at $f_2 - 0.000794$ with an equal amplitude to that of f_2 within the theoretic limit frequency resolution of 0.0009656 d^{-1} but over the adopted smallest resolvable spacing of 0.000449 d^{-1} . This could be an indication of rotation other than a pulsational peak. Then, $f_2, f_4, f_5, 3f_2$ are probably caused by the rotation of the star. On the other hand, f_0, f_1 and $f_7 = 1.2517 \text{ d}^{-1}$ seem to be independent pulsational peaks of the GDOR type, regarding the temperature $T_{\text{eff}} \sim 7100 \text{ K}$ of this star located in the region of GDOR pulsators. The peak $f_3 = 7.287296 \text{ d}^{-1}$ seems to be an isolated pulsational DSCT peak. In the residuals of Fig. 6, it seems there are three other peaks in the range higher than 5.0 d^{-1} . They are probably other three independent peaks of DSCT pulsation. So a conclusion may be drawn that HD 53349 is a hybrid δ Sct and γ Dor pulsator superimposed with spots rotational variability (Rodríguez, 2023).

It is noteworthy that the above alternative rotational interpretation of light variability for the two stars HD 53166 and HD 63349 had assumed larger errors in the resolved frequencies, which are actually at least two times the effective frequency resolution and ignored a frequency difference 39 times ($0.003/0.000076$) the calculated errors in frequencies, even though the possible explanation is coincidentally conform with the classification in Balona (2022a). The author believe in the effective frequency resolution using 24 *TESS* sectors data, the frequency difference two times higher than its value and far beyond frequency errors cannot be ignored. The frequencies values and measurement uncertainties have been carefully evaluated. Therefore the author prefers to take the hybrid δ Sct and γ Dor pulsators identification as final conclusion.

The matter of true intrinsic variables of these two comparison stars demonstrated the power of *TESS* data. *TESS* data with 27.4 days time coverage in a sector, are especially suitable for detecting γ Dor-type pulsations – γ Dor light curves on a *TESS* sector are good enough for visual inspection on a computer screen. Previous short-term poor-quality ground observations in the literature might have misled to inaccurate resolution of light variations. This implies a clue applying *TESS* data to stars with less photometry and puzzle results in the literature.

A further search for γ Dor stars in an extended sky region centered on HD 52788 is underway.

5.3. H-R Diagrams

Taking advantage of those recently released catalogs of δ Sct stars by various all-sky surveys, we can draw the three stars against those published known sources in the Hertzsprung-Russell diagrams for comparison. There are quite a big volume of known δ Sct stars to compare with: (1) General Catalog of Variable Stars (GCVS database, Version 2022.09 V5.2, Samus et al. 2017)⁹ designated 1018 DSCT; 267 SXPHE; (2) the International Variable Stars Index (VSX) database of AAVSO (Watson et al., 2022, 2006)¹⁰ collected 27 194; (3) 3939 DSCT were published in ASAS-SN Catalog of Variable Stars X (Christy et al., 2022)¹¹; ASAS-SN also listed 2231 HADS; (4) 24 488 contained in OGLE-IV (Soszyński et al., 2021; Pietrukowicz et al., 2020)¹²; (5) 16 709 published in ZTF (Bellm et al., 2019; Masci et al., 2019; Ofek et al., 2020; Chen et al., 2020)¹³; (6) ASAS-3 listed 3538; (7) Simbad archived 8440; (8) 14 042 DSCT identified using TESS data by Balona and Ozuyar (2020) and Balona (2022a); etc. After removal of the duplicate stars among these catalogs, we reached a number of 70 552 δ Sct stars from the above sources.

Using *Gaia* DR2 and DR3 *G, BP, RP* magnitude results (*Gaia* Collaboration et al., 2022, 2016), a *Gaia* color-magnitude diagram of δ Sct stars is drawn in Fig. 7.

We further extracted effective temperature, luminosity, surface gravity, parallax, distance and other stellar parameters from *TESS* Input Catalog (TIC v8.2, Paegert et al., 2021) and *Gaia* DR2/DR3 for the collection. However, a good number of δ stars from the above surveys have less luminosities than the Sun, we instead tend to draw additional H-R diagrams only for those δ Sct stars collected in Simbad rather than VizieR. It is known that Simbad/CDS provides information on astronomical objects which have been studied in scientific articles, while the CDS VizieR database is a complementary research tool which is composed of various survey catalogs. Figures 8–9 show the three stars compared with 8440 δ Sct stars extracted from Simbad (as of September 2022). As shown, even only the Simbad 8440 δ Sct stars, there are still considerable number with

⁹online URL: <http://www.sai.msu.su/gcvs/cgi-bin/search.htm#cat>

¹⁰<https://www.aavso.org/vsx/>

¹¹Christy et al., 2022, MNRAS, in press: <https://asas-sn.osu.edu/variables>

¹²<https://ogledb.astrouw.edu.pl/ogle/OCVS/>

¹³Zwicky Transient Facility: <https://www.ztf.caltech.edu/>

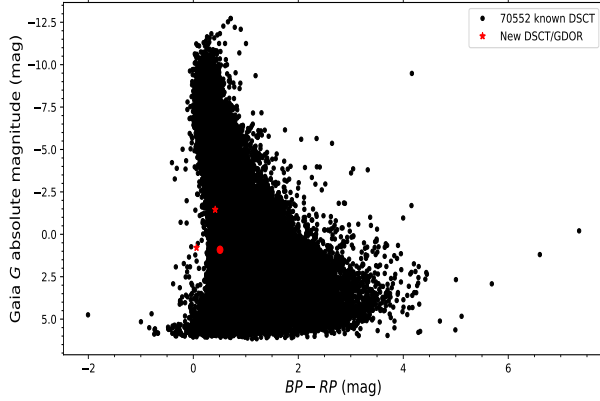


Figure 7: Present δ Sct stars in *Gaia* color-magnitude diagram, plotted contrast with the known 70 552 DSCT collected from several sources including but not limited to Simbad, GSVC, VSX, OGLE, ASAS-3, ASAS-SN, ZTF, etc. HD 52788 in red dot.

lower luminosities and effective temperatures than solar values. If all collected DSCT were used, the H-R diagrams would show a much extended DSCT domain than the classical borders that demonstrated in the literature (see fig.1 in Handler, 2009b; Jeffery, 2008; Rodríguez and Breger, 2001; Breger, 2000) and in the recent studies of a sample of 15 000+ *Kepler* A and F stars in and around the δ Scuti instability strip using *Gaia* DR2 parallaxes by Murphy et al. (2019).

Similarly, we have collected γ Dor stars from multiple sources: (1) dozens from earlier pioneering works (Henry et al., 2007, 2005; Kaye et al., 1999); (2) 120+ from Henry et al. (2022, 2011); (3) 611 and 207 resulted from *Kepler* data by Li et al. (2020b) and Bradley et al. (2015), respectively; (4) 108 in GCVS v5.2 (as of 2022 Oct.19); (5) 1032 in VSX-AAVSO (as of 2022 Nov.15); (6) 1641 in Simbad (as of 2022 Nov.15); (7) 6358 based on TESS data identified by Balona (2022a) and Balona and Ozuyar (2020); etc. After removal of the duplicate stars among these sources, we reached a number of 8 080 γ Dor stars with stellar parameters extracted from *Gaia* DR2/DR3 and TIC v8.2. A H-R diagram of γ Dor stars is then drawn in Fig. 10, where 8080 GDOR from the above sources were used.

It is noted that both DSCT and GDOR domains are much extended to lower luminous region. This bias with classical ranges probably be resulted either from inaccurate parameters or false memberships of each type stars. In this regard, a further examination and confirmation of bona fide members of each one of DSCT and GDOR in the mixed collections is urgently needed. For instance, Bradley et al. (2015) found 207 γ Dor candi-

dates and 84 δ Sct candidates from *Kepler* data. These candidates could have been taken as true members in some relevant catalogs – a duplication check shows 125 of 207 being collected in other publications. The star BS 8799 (=HD 218396 =TIC 245368902=V342 Peg) in Kaye et al. (1999)’s confirmed list of GDOR, its variability type is controversial as Simbad labels it to be an ellipsoidal variable other than GDOR. However, it is a genuine GDOR, *TESS* data on sector 56 (2022.09.02) show clearly typical γ Dor-type light variations. Those discoveries resulted from automatic identification using machine learning methods based on large sky surveys are huge and would have mixed with some non-members. The author is thus inspired to examine and verify the candidates of various sources with *TESS* data in a up-coming work.

On the other hand, Balona and Ozuyar (2020) and Balona (2022b) who have carefully chosen and calibrated effective temperature in sample stars to ensure a safe variability classification. The spectral type directly related to temperature is important for ascertaining the variability class. Rigorous observational H-R diagrams for both δ Sct and γ Dor bona fide members based on reliable temperature and luminosity by taking account of *Gaia* DR3 parameters corrected for interstellar extinction would be much persuasive and meaningful. With such convincing H-R diagrams we can compare them with theoretic borders of instability strip connecting to oscillation mechanisms of δ Sct and γ Dor stars such as that by Dupret et al. (2005) and Xiong et al. (2016).

The author would like to conduct an asteroseismology for these three stars upon making relevant stellar evolution and oscillation modeling programs available to run in the near future. At present we report the full analysis of light curves and the results of new discoveries of pulsational variability of HD 53166 and HD 53349, and a complete update of HD 52788 light variations complexity.

This manuscript was prepared following ‘elsarticle-template-harv.tex’

Acknowledgements

I appreciate the two anonymous referees for their thoughtful comments and meticulous reading which al-

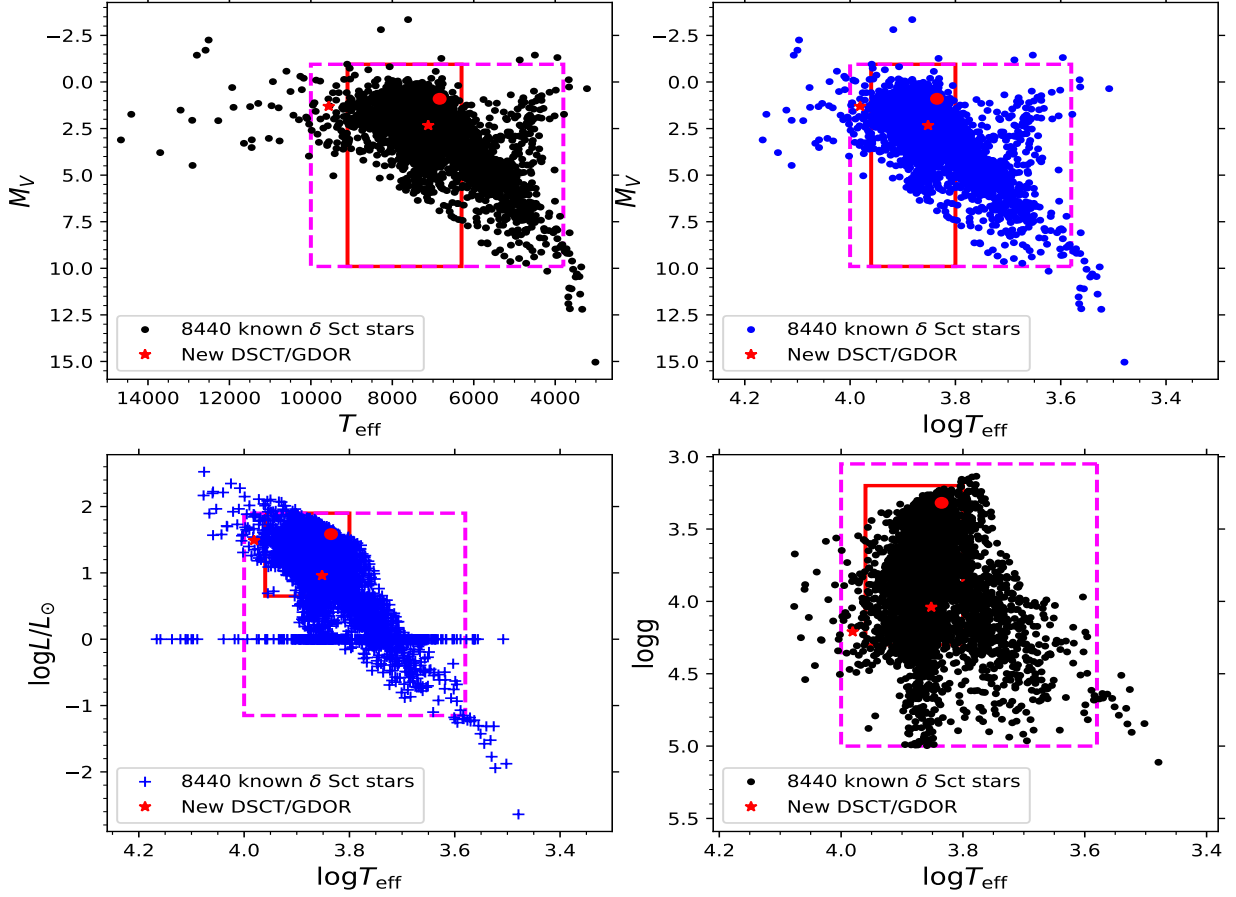


Figure 8: Newly discovered pulsating variable stars of δ Sct (red asterisks) and HD 52788 (red dot) plotted contrast with the known 8440 DSCT extracted from Simbad. Red squares refer to classical δ Sct domain: T_{eff} in [6300, 9100], $\log T_{\text{eff}}$ in [3.80, 3.96], $\log g$ in [3.2, 4.3], $\log L/L_{\odot}$ in [0.65, 1.90] consistent with the H-R diagram of pulsators given by Handler (2009b); Jeffery (2008); Breger (2000); magenta dashed squares refer to an extended domain: T_{eff} in [3800, 10000], $\log T_{\text{eff}}$ in [3.58, 4.00], $\log g$ in [3.05, 5.0], $\log L/L_{\odot}$ in [-1.15, 1.90], M_V in [9.9, -0.95]. Note: δ Sct domain is explicitly much enlarged might be due to inaccurate stellar parameters in databases, especially lower luminosities and effective temperatures than the solar values ($\log L/L_{\odot} < 0$ and $\log T_{\text{eff}} < 3.76$, $T_{\text{eff}} < 5780$ K).

lowed the author to greatly improve the quality of the manuscript. I am indebted to my wife for her unwavering support throughout my research. This work could not have been done without my wife's continuous support. This paper includes data collected with the *TESS* mission. Funding for the *TESS* mission is provided by the NASA Explorer Program. *TESS* data were obtained from the MAST data archive at the Space Telescope Science Institute (STScI). STScI is operated by the Association of Universities for Research in Astronomy, Inc., under NASA contract NAS 5-26555. We acknowledge the use of *TESS* data, which are de-

rived from pipelines at the *TESS* Science Processing Operations Center (SPOC). *TESS* High Level Science Products (HLSP) produced by the Quick-Look Pipeline (QLP) at the *TESS* Science Office at MIT, which are publicly available from the Mikulski Archive for Space Telescopes (MAST). This research has made use of the SIMBAD/VizieR databases, operated at CDS, Strasbourg, France. This research has made use of the International Variable Star Index (VSX) database, operated at AAVSO, Cambridge, Massachusetts, USA. Special acknowledgements go to all the projects and surveys mentioned in this work including but not limited

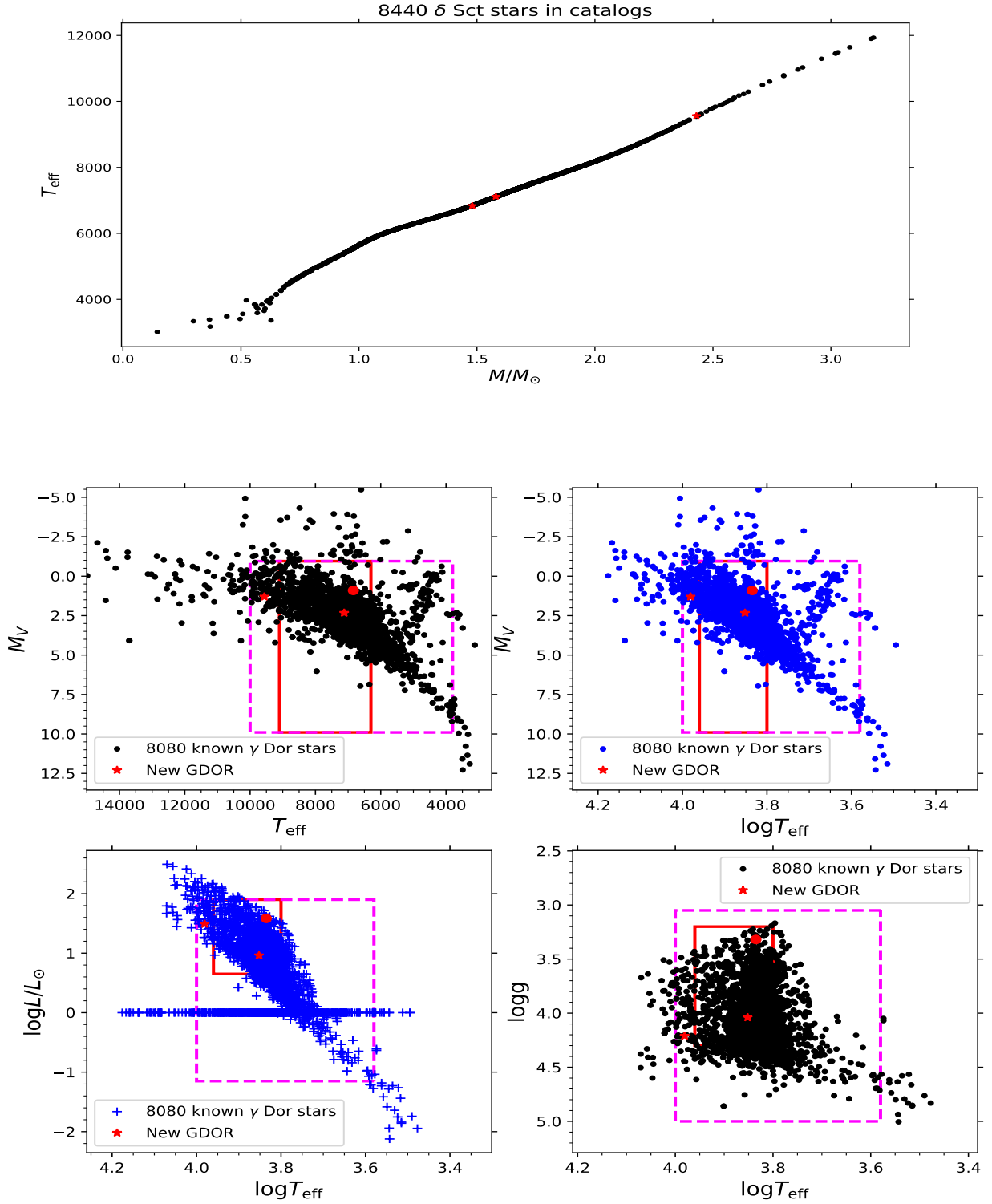


Figure 10: Newly discovered pulsating variable stars of γ Dor– δ Sct hybrid (red asterisks) and HD 52788 (red dot) plotted contrast with the known 8080 GDOR. The same squares as Fig. 8. Note: γ Dor domain is explicitly much enlarged might be due to inaccurate stellar parameters in databases, especially lower luminosities and effective temperatures than the solar values ($\log L/L_{\odot} < 0$ and $\log T_{\text{eff}} < 3.76$, $T_{\text{eff}} < 5780$ K).

to: OGLE-V, ASAS-3, ASAS-SN, and ZTF. This work has made use of data from the European Space Agency (ESA) mission *Gaia* (<https://www.cosmos.esa.int/gaia>), processed by the *Gaia* Data Processing and Analysis

Consortium (DPAC¹⁴). Funding for the DPAC has been provided by national institutions, in particular the in-

¹⁴<https://www.cosmos.esa.int/web/gaia/dpac/consortium>

stitutions participating in the *Gaia* Multilateral Agreement. This work made use of *Astropy*:¹⁵ a community-developed core Python package and an ecosystem of tools and resources for astronomy (Astropy Collaboration et al., 2013, 2018, 2022); *Astroquery* (Ginsburg et al., 2019); *Lightcurve* (The Astropy Collaboration et al., 2018b); *Matplotlib* (Hunter, 2007); *SciPy* (Virtanen et al., 2020); *NumPy* (Harris et al., 2020).

Appendix A. A Catalog of 70552 δ Scuti Stars

Based on δ Sct stars listed in several existing catalogs and databases by Simbad, OGLE, VSX, ASAS-SN, ZTF, GCVS, and other sources including three dozen sporadic new DSCTs picked up from recent publications (e.g. Kirmizitas et al. 2022; Shi et al. 2021b) and 14042 DSCT from *TESS* data by Balona and Ozuyar (2020); Balona (2022a), we reached an up-to-date comprehensive catalog of δ Sct stars that consists of 70 552 individual stars after removing those duplicated entries. For those 14042 DSCT, the main identifiers if available in Simbad were extracted and compiled in the list. In fact, there are 9091, 706 and 1559 with HD, BD and TYC identifiers, respectively.

Each entry in the catalog is comprised of 26 columns: TIC, source ID or main ID of Simbad, *Gaia* DR3 ID, RA_Dec/2MASS_ID, *B*_TIC, *V*_TIC, T_{eff} _TIC, T_{eff} _Gaia, $\log g$ _TIC, $\log g$ _Gaia, Mass_TIC, *R*_TIC, *R*_Gaia, *L*_TIC, *L*_Gaia, parallax(mas), distance(pc), M_V , $\log T_{\text{eff}}$ _TIC, $\log L$ _TIC, *G*_mag, *BP*_mag, *RP*_mag, *BP* – *RP*, *BP* – *G*, *G* – *RP*, Radial_Velocity_Gaia and errors for a few parameters.

The whole catalog in its entirety is provided as online materials in both machine-readable text format (CSV file) and human-friendly HTML version¹⁶. Interested readers may enquire it from the author via email or download full table in CSV file on the journal's web or <https://deltascuti.wixsite.com/delta/download>. A reduced demo is given in Table A.1. More importantly, in the HTML version, each TIC ID is hyperlinked to STScI archive MAST in a default radius of 0.00033° of the target, each *Gaia* DR3 ID with hyperlink to *Gaia* data at VizieR/CDS, and main IDs or coordinates are linked to CDS Portal. The HTML version makes consulting, checking, follow-up and downloading *TESS/Kepler/K2* and *Gaia* DR3 data unprecedentedly convenient and efficient.

Appendix B. A Catalog of 8080 γ Doradus Stars

We have compiled a catalog of γ Dor stars based on the sources of GCVS, VSX, *Kepler* data (Li et al., 2020b), Henry et al. (2022, 2011, 2007), Simbad, a few thousand from *TESS* (Balona and Ozuyar, 2020; Balona, 2022a) and others. After removal of the duplicate stars among these sources, we reached a number of 8080 individual γ Dor stars with stellar parameters extracted from *Gaia* DR2/DR3 and TIC v8.2. Parameters or columns are the same as the above δ Sct stars catalog. The whole catalog in its entirety is provided as online materials in a machine-readable text format (CSV file). Interested readers may request it from the author via email or download on the journal's web or <https://deltascuti.wixsite.com/delta/download>. A reduced demo is given in Table A.2.

¹⁵<http://www.astropy.org>

¹⁶<https://deltascuti.wixsite.com/delta/catalog>

Table 4: Frequency solution of HD 52788 (=TIC 279361762) based on all available *TESS* data secured in 24 Sectors. The digits in parentheses represent the error in the last one or two decimal places. Amplitude in mmag and errors in amplitudes are 5.96 ppm.

Frequency (d^{-1})	Amplitude	Phase (0-1)	SNR
$f_0=10.760712(1)$	3.757	0.6532(3)	299.1
$f_1=8.912941(1)$	3.336	0.4876(3)	208.7
$f_2=6.718369(1)$	3.145	0.5542(4)	233.8
$f_3=8.322361(1)$	2.863	0.0899(3)	193.2
$f_4=7.361251(2)$	2.730	0.5630(6)	191.2
$f_5=9.667860(3)$	2.711	0.6036(9)	188.3
$f_6=7.625737(2)$	1.647	0.4090(6)	109.2
$f_7=9.827841(2)$	1.635	0.0752(7)	113.6
$f_8=5.891104(2)$	1.634	0.9169(6)	142.2
$f_9=9.940035(3)$	1.520	0.5681(8)	105.6
$f_{10}=5.692326(3)$	1.507	0.3937(9)	131.2
$f_{11}=8.912464(3)$	1.483	0.5398(7)	92.7
$f_{12}=8.139382(2)$	1.330	0.0989(7)	89.8
$f_{13}=9.197316(2)$	1.324	0.7725(7)	84.2
$f_{14}=6.072851(2)$	1.311	0.0325(6)	105.1
$f_{15}=6.816985(3)$	1.264	0.1831(7)	94.0
$f_{16}=10.301894(3)$	1.257	0.0196(8)	89.7
$f_{17}=6.828059(4)$	1.200	0.4087(11)	89.2
$f_{20}=5.434878(3)$	1.012	0.1317(10)	94.3
$f_{21}=8.546385(2)$	0.980	0.9524(6)	61.3
$f_{23}=7.260373(3)$	0.968	0.7540(9)	67.8
$f_{25}=7.059142(5)$	0.897	0.8382(16)	62.8
$f_{27}=9.512210(7)$	0.799	0.5763(22)	55.5
$f_{28}=7.772967(15)$	0.754	0.6716(44)	50.0
$f_{30}=7.575876(4)$	0.693	0.4292(12)	45.9
$f_{31}=4.954131(6)$	0.687	0.4062(19)	67.8
$f_{32}=8.032471(4)$	0.686	0.7784(11)	46.3
$f_{33}=9.598536(7)$	0.678	0.6018(21)	47.1
$f_{34}=8.425755(4)$	0.609	0.2449(12)	41.1
$f_{35}=11.284097(6)$	0.544	0.4131(17)	44.9
$f_{36}=6.786902(6)$	0.540	0.3683(18)	40.1
$f_{37}=7.834032(5)$	0.494	0.2679(14)	32.7
$f_{38}=9.269924(7)$	0.479	0.9459(20)	30.4
$f_{39}=9.515054(7)$	0.466	0.2663(20)	32.4
$f_{41}=9.743959(11)$	0.430	0.7088(315)	29.8
$f_{42}=4.386572(7)$	0.428	0.0939(22)	44.2
$f_{43}=9.191466(8)$	0.424	0.2348(22)	27.0
$f_{44}=5.130545(5)$	0.409	0.4008(14)	38.1
$f_{45}=5.133285(8)$	0.404	0.3003(23)	37.6
$f_{46}=10.772772(8)$	0.396	0.6975(24)	31.5
$f_{47}=4.919064(8)$	0.395	0.2621(23)	38.9
$f_{48}=11.428913(8)$	0.392	0.3759(24)	32.4
$f_{49}=9.510808(8)$	0.381	0.1872(25)	26.4
$f_{50}=5.156588(9)$	0.368	0.5539(26)	34.3

Table 4: — Continued

Frequency (d^{-1})	Amplitude	Phase (0-1)	SNR
$f_{51}=6.001676(9)$	0.364	0.9169(26)	29.2
$f_{52}=7.256143(9)$	0.361	0.2173(26)	25.3
$f_{53}=5.540744(9)$	0.340	0.9782(28)	29.6
$f_{54}=8.657510(10)$	0.339	0.3604(28)	21.2
$f_{55}=8.613910(10)$	0.313	0.2644(31)	19.6
$f_{56}=10.271927(10)$	0.309	0.7930(31)	22.0
$f_{57}=9.458759(11)$	0.303	0.4938(31)	19.3
$f_{58}=7.245365(11)$	0.303	0.1817(32)	21.2
$f_{59}=11.281291(10)$	0.302	0.6374(31)	25.0
$f_{60}=5.906064(11)$	0.291	0.8418(32)	25.3
$f_{61}=7.184681(11)$	0.287	0.1920(33)	20.1
$f_{62}=9.905449(11)$	0.278	0.8832(34)	19.3
$f_{63}=11.285506(11)$	0.278	0.7845(34)	22.9
$f_{64}=9.908260(12)$	0.269	0.6558(35)	18.7
$f_{65}=6.233235(12)$	0.265	0.2720(36)	21.3
$f_{66}=7.286575(12)$	0.263	0.6753(36)	18.4
$f_{67}=5.393172(12)$	0.255	0.9920(37)	23.8
$f_{68}=8.661686(13)$	0.251	0.0729(38)	15.7
$f_{69}=8.663166(13)$	0.242	0.3133(40)	15.1
$f_{70}=9.741146(13)$	0.238	0.9258(40)	16.6
$f_{71}=5.330562(14)$	0.235	0.7490(40)	21.9
$f_{72}=9.745367(14)$	0.233	0.0881(41)	16.2
$f_{73}=8.350984(14)$	0.226	0.4041(42)	15.2
$f_{74}=11.431706(8)$	0.216	0.1647(24)	17.9
$f_{75}=11.427492(16)$	0.201	0.0345(47)	16.6
$f_{76}=6.821376(16)$	0.196	0.0796(49)	14.6
$f_{77}=10.363481(17)$	0.191	0.7322(49)	13.6
$f_{78}=8.101823(17)$	0.187	0.2150(51)	12.6
$f_{79}=2.833634(18)$	0.180	0.5280(52)	15.0
$f_{80}=9.552320(18)$	0.175	0.3082(55)	12.1
$f_{81}=5.304389(19)$	0.167	0.4670(56)	15.5
$f_{82}=7.393222(19)$	0.167	0.1204(56)	11.7
$f_{83}=6.911048(20)$	0.159	0.1184(59)	11.8
$f_{84}=10.233948(22)$	0.145	0.1224(65)	10.4
$f_{85}=10.236667(22)$	0.145	0.0489(66)	10.3
$f_{86}=6.573550(22)$	0.143	0.8390(65)	10.6
$f_{87}=8.035146(23)$	0.139	0.9151(68)	9.4
$f_{88}=6.305248(23)$	0.138	0.5002(68)	11.1
$f_{89}=9.517827(23)$	0.136	0.6075(69)	9.5
$f_{90}=13.292368(24)$	0.135	0.1017(70)	12.2
$f_{91}=8.654768(24)$	0.130	0.9650(71)	8.1
$f_{92}=18.304428(25)$	0.126	0.3905(74)	13.0
$f_{93}=7.838867(25)$	0.125	0.7913(75)	8.3
$f_{95}=8.211857(26)$	0.124	0.1116(77)	8.3
$f_{96}=12.925388(26)$	0.123	0.3218(78)	11.0
$f_{97}=8.107359(26)$	0.122	0.4421(77)	8.2
$f_{98}=8.105974(26)$	0.121	0.0219(76)	8.2
$f_{100}=19.184598(27)$	0.119	0.5267(81)	13.3

Table 4: — Continued

Frequency (d ⁻¹)	Amplitude	Phase (0-1)	SNR
$f_{101}=7.565613(27)$	0.118	0.0656(80)	7.8
$f_{102}=10.552950(27)$	0.117	0.8282(81)	9.3
$f_{103}=4.487832(27)$	0.117	0.8186(81)	12.1
$f_{104}=9.029008(27)$	0.115	0.2003(81)	7.3
$f_{105}=13.577598(28)$	0.113	0.5387(84)	11.0
$f_{106}=14.213484(28)$	0.111	0.1584(85)	11.0
$f_{107}=19.313794(30)$	0.106	0.6342(89)	11.8
$f_{108}=3.516773(31)$	0.103	0.3656(93)	10.6
$f_{109}=6.346939(31)$	0.102	0.0902(93)	8.1
$f_{110}=17.029084(34)$	0.097	0.4436(100)	11.0
$f_{112}=9.902661(34)$	0.094	0.608(10)	6.6
$f_{113}=7.280701(35)$	0.092	0.170(11)	6.4
$f_{114}=5.124742(35)$	0.091	0.246(11)	8.5
$f_{115}=7.190440(36)$	0.090	0.944(11)	6.3
$f_{116}=10.403170(36)$	0.087	0.412(11)	6.2
$f_{117}=14.603881(37)$	0.087	0.262(11)	8.9
$f_{118}=17.990261(36)$	0.086	0.872(11)	9.1
$f_{119}=7.931700(38)$	0.082	0.469(12)	5.4
$f_{120}=8.320538(38)$	0.082	0.353(11)	5.5
$f_{122}=20.274321(41)$	0.081	0.286(12)	13.0
$f_{123}=9.461381(40)$	0.080	0.145(12)	5.1
$f_{124}=18.411317(47)$	0.076	0.992(14)	7.9
$f_{125}=9.452980(42)$	0.075	0.797(13)	4.8
$f_{126}=10.784904(44)$	0.074	0.361(13)	5.9
$f_{127}=7.258622(46)$	0.070	0.045(14)	4.9
$f_{128}=18.580695(47)$	0.069	0.630(14)	7.2
$f_{129}=7.363065(49)$	0.069	0.933(15)	4.8
$f_{130}=9.602568(50)$	0.063	0.661(15)	4.4
$f_{131}=10.771011(51)$	0.062	0.099(15)	5.0
$f_{132}=20.195160(59)$	0.058	0.965(17)	9.4
$f_{133}=6.575096(57)$	0.058	0.866(17)	4.3

Frequencies under resolving limit and combination terms*

$f_{18}=f_5+0.000077=9.667937(3)$	1.152	0.2479(10)	80.0
$f_{19}=f_9-0.000078=9.939957(3)$	1.120	0.2602(8)	77.8
$f_{22}=f_0+0.000410=10.761122(1)$	0.973	0.1426(3)	77.5
$f_{24}=f_{23}+0.000013=7.260386(3)$	0.946	0.2253(9)	66.2
$f_{26}=f_6+0.000273=7.626010(5)$	0.894	0.6858(14)	59.3
$f_{29}=f_7-0.000116=9.827725(5)$	0.693	0.6135(14)	48.2
$f_{40}=f_{33}-0.000042=9.598494(7)$	0.448	0.1664(21)	31.1
$f_{99}=f_{25}-0.000338=7.058804(26)$	0.120	0.7787(78)	8.4
$f_{134}=f_{51}+0.000268=6.001944(55)$	0.057	0.665(16)	4.6
$f_{94}=f_3+f_4-0.000079=15.683533$	0.125	0.984184	13.8
$f_{111}=f_0+f_1-0.000122=19.673531$	0.095	0.851158	12.5
$f_{121}=2f_0-0.000011=21.521412$	0.081	0.819591	21.1

Zeropoint: 7.81185449 mag

Residuals: 0.00273008 mag

Table 5: Frequency solution of HD 53166 (=TIC 279431011) based on 24 *TESS* sectors 2–13 and 27–39. A frequency term within the frequency resolution 0.00152068 d⁻¹ relative to one of the harmonics of the main frequencies or their combinations will be taken as real, otherwise an independent frequency. Digits in parentheses refer to errors in the last decimal place. Amplitude in mmag and errors in amplitudes are 2.02 ppm.

Frequency (d ⁻¹)	Amplitude	Phase (0-1)	SNR
$f_0=0.85999(1)$	0.326	0.265(1)	19.8
$f_1=2.48885(1)$	0.307	0.804(1)	44.27
$f_3=0.85698(3)$	0.120	0.250(3)	7.30
$f_2=2f_1-0.000126$	0.301	0.297	78.67
$f_4=2f_0+0.003006$	0.049	0.921	5.84
$f_5=3f_1-0.000203$	0.028	0.752	11.32
$f_6=4f_1-0.000344$	0.023	0.139	10.41
$f_7=5f_1-0.000203$	0.018	0.916	7.80
$f_8=6f_1-0.000595$	0.016	0.509	6.84
Zeropoint: -4.43230403e-06 mag			
Residuals: 0.000590436668 mag			

Table 6: Frequency solution of HD 53349 (=TIC 279476396) Based on 24 *TESS* sectors data. Digits in parentheses refer to errors in the last two decimal places. Errors in amplitudes are 0.42 ppm.

Frequency (d ⁻¹)	Amplitude (mmag)	Phase (0-1)	SNR
$f_0=1.888139(05)$	0.039	0.4767(17)	24.90
$f_1=1.809503(06)$	0.035	0.2293(19)	22.35
$f_2=1.538036(12)^*$	0.018	0.0002(36)	11.58
$f_3=7.287296(23)$	0.009	0.7736(72)	9.57
$f_4=6.148190(26)$	0.008	0.1311(79)	8.34
$f_5=3.074502(27)$	0.008	0.4585(82)	6.43
Zeropoint: 4.43898411e-07 mag			
Residuals: 0.000186609086 mag			

Accompanied with an equal amplitude peak at $f_2-0.000794$, separated over the adopted empirical frequency resolution of 0.000449 d⁻¹, but within the theoretic frequency resolution of 0.0009656 d⁻¹.

Table A.1: A combined catalog of 70,552 δ Sc stars (reduced demo version). Full table in CSV file is on the journal's web or <https://delatascuti.wixsite.com/delta/download>.

TIC ID	Source ID	Gaia DR3	2MASS/RA-Dec	B-TIC	V-TIC	$T_{\text{eff-TIC}}$	$T_{\text{eff-Gaia}}$	$\log g_{\text{TIC}}$	$\log g_{\text{Gaia}}$
TIC 1000089523	ZTF141934.31+113547.9	1225642756991957120	214.892981 11.596656	nan	18.6731	nan	7297.78	nan	4.3895
TIC 1000101652	ZTF140848.41+123606.6	1226608196920814848	212.201759 12.601821	nan	18.4599	7019.0	7150.74	nan	4.5852
TIC 1000104768	ZTF141805.41+131126.6	1226865933613176448	214.522574 13.19073	nan	17.5211	6977.0	6847.88	4.80123	4.469
TIC 100012164	TIC 100012164	864002769753103616	173.268106 63.89601	9.552	9.253	7376.0	7211.87	4.09371	3.9797
TIC 1000156752	ZTF135719.50+152149.3	1231155948812038016	209.331291 15.363725	nan	18.7852	nan	7277.38	nan	4.3927
TIC 1000164869	ZTF141730.31+150946.1	123187678683202816	214.376322 15.162809	nan	18.897	nan	7405.75	nan	4.4463
TIC 99968017	ZTF1192910.74071936.8	4207666832973112960	292.294793 -7.326884	15.583	15.469	6987.0	7740.32	4.10928	4.1564
TIC 99971924	ZTF1112629.01+612732.7	862543889621373696	171.621022 61.459218	14.933	15.045	7537.0	7441.75	4.36968	3.9848
TIC 99978409	ZTF1204145.78+334207.8	1863327001102874240	310.440792 33.702168	15.369	14.673	6938.0	9015.28	3.30249	3.5687
TIC 99983100	ASASSN-V J204212.17+323517.2	1863120877024811264	20.42 12.17 +32 35 17.2	nan	15.7216	5886.0	5831.14	3.32024	4.0683
TIC 99995027	HD 175355	4310238314231510528	283.67868 8.099308	9.366	9.142	8111.0	8395.73	4.26642	4.2661

Table A.2: A combined catalog of 8080 γ Dor stars (reduced demo version). Full table in CSV file is on the journal's web or <https://delatascuti.wixsite.com/delta/download>.

TIC ID	Source ID	Gaia DR3	2MASS/RA-Dec	B-TIC	V-TIC	$T_{\text{eff-TIC}}$	$T_{\text{eff-Gaia}}$	$\log g_{\text{TIC}}$	$\log g_{\text{Gaia}}$	Mass-TIC
TIC 100008712	TIC 100008712	86368349963563648	J112953.36+630613.9	10.129	9.83	7080.0	6946.84	4.27086	4.1372	1.57
TIC 100102390	HD 10167	4958910970141833216	J013830.73+425540.6	6.984	6.67	7008.68	nan	3.8645	nan	1.54
TIC 1001512783	TIC 153989642	1685166397526839424	-	nan	8.7316	6308.0	6187.54	nan	4.2671	nan
TIC 1002938519	TIC 379081616	3726490479878642688	-	nan	5.5506	nan	nan	nan	nan	nan
TIC 100325374	TIC 100325374	6668210166134920192	J202832.56+484039.2	9.62	9.242	7070.0	6913.17	4.11936	4.0608	1.56
TIC 100378749	TIC 100378749	6474064587655163776	J203049.99+525234.2	9.489	9.077	6660.0	6554.4	4.20033	4.1194	1.4
TIC 99842485	TIC 99842485	1054696912513345280	J110332.30+625725.2	9.705	9.293	6376.0	nan	nan	nan	nan
TIC 99867019	TIC 99867019	861500899763587456	J110535.22+60247.8	10.144	9.688	6488.0	nan	nan	nan	nan
TIC 99883676	TIC 99883676	4200367450155720960	J1192812.96+093216.8	8.679	8.38	7130.0	7023.34	4.2454	4.1323	1.587
TIC 99898937	TIC 99898937	862289764996484096	J110913.24+622951.8	9.537	9.259	7477.0	7408.35	4.19653	4.1017	1.72
TIC 99971569	TIC 99971569	863973357816605440	J112609.67+634936.5	9.278	8.968	7158.0	6999.44	3.92968	3.9323	1.6

Note: References with 5+ authors may be cutoff and replaced by ‘et al.’ in this manuscript.

References

- Aerts, C., 2021. Probing the interior physics of stars through asteroseismology. *Reviews of Modern Physics* 93, 015001. doi:10.1103/RevModPhys.93.015001, arXiv:1912.12300.
- Antoci, V., Cunha, M.S., Bowman, D.M., Murphy, S.J., Kurtz, D.W., Bedding, T.R., Borre, C.C., Christophe, S., Szabó, R., et al., 2019. The first view of δ Scuti and γ Doradus stars with the TESS mission. *MNRAS* 490, 4040–4059. doi:10.1093/mnras/stz2787, arXiv:1909.12018.
- Astropy Collaboration, Price-Whelan, A.M., Lim, P.L., Earl, N., Starkman, N., Bradley, L., Shupe, D.L., Patil, A.A., Corrales, L., Brasseur, C.E., et al., Astropy Project Contributors, 2022. The Astropy Project: Sustaining and Growing a Community-oriented Open-source Project and the Latest Major Release (v5.0) of the Core Package. *ApJ* 935, 167. doi:10.3847/1538-4357/ac7c74, arXiv:2206.14220.
- Astropy Collaboration, Price-Whelan, A.M., Sipőcz, B.M., Günther, H.M., Lim, P.L., Crawford, S.M., Conseil, S., Shupe, D.L., Craig, M.W., Woillez, J., et al., Astropy Contributors, 2018. The Astropy Project: Building an Open-science Project and Status of the v2.0 Core Package. *AJ* 156, 123. doi:10.3847/1538-3881/aabc4f, arXiv:1801.02634.
- Astropy Collaboration, Robitaille, T.P., Tollerud, E.J., Greenfield, P., Droettboom, M., Bray, E., Aldcroft, T., Davis, M., Ginsburg, A., Price-Whelan, A.M., et al., 2013. Astropy: A community Python package for astronomy. *A&A* 558, A33. doi:10.1051/0004-6361/201322068, arXiv:1307.6212.
- Astudillo-Defru, N., Cloutier, R., Wang, S.X., Teske, J., Brahm, R., Hellier, C., Winters, J.G., et al., 2020. A hot terrestrial planet orbiting the bright M dwarf L 168-9 unveiled by TESS. *A&A* 636, A58. doi:10.1051/0004-6361/201937179, arXiv:2001.09175.
- Balona, L.A., 2014. Mode density and frequency extraction in the δ Scuti star HD 50844. *MNRAS* 439, 3453–3460. doi:10.1093/mnras/stu193, arXiv:1402.0803.
- Balona, L.A., 2022a. Identification and classification of TESS variable stars. arXiv e-prints, arXiv:2212.10776arXiv:2212.10776.
- Balona, L.A., 2022b. Rapidly oscillating TESS A-F main-sequence stars: are the roAp stars a distinct class? *MNRAS* 510, 5743–5759. doi:10.1093/mnras/stac011, arXiv:2109.02246.
- Balona, L.A., Daszyńska-Daszkiewicz, J., Pamyatnykh, A.A., 2015. Pulsation frequency distribution in δ Scuti stars. *MNRAS* 452, 3073–3084. doi:10.1093/mnras/stv1513, arXiv:1505.07216.
- Balona, L.A., Krisciunas, K., Cousins, A.W.J., 1994. Gamma Doradus : evidence for a new class of pulsating star. *MNRAS* 270, 905–913. doi:10.1093/mnras/270.4.905.
- Balona, L.A., Ozuyar, D., 2020. Pulsation among TESS A and B stars and the Maia variables. *MNRAS* 493, 5871–5879. doi:10.1093/mnras/staa670, arXiv:2001.04497.
- Battley, M.P., Kunitomo, M., Armstrong, D.J., Pollacco, D., 2021. Revisiting the Kepler field with TESS: Improved ephemerides using TESS 2 min data. *MNRAS* 503, 4092–4104. doi:10.1093/mnras/stab701, arXiv:2103.03259.
- Bellm, E.C., Kulkarni, S.R., Graham, M.J., Dekany, R., Smith, R.M., Riddle, R., Masci, F.J., Helou, G., Prince, T.A., Adams, S.M., Barbarino, C., Barlow, T., Yan, L., et al., 2019. The Zwicky Transient Facility: System Overview, Performance, and First Results. *PASP* 131, 018002. doi:10.1088/1538-3873/aacbc6, arXiv:1902.01932.
- Bowman, D.M., Kurtz, D.W., 2014. Pulsational frequency and amplitude modulation in the δ Scuti star KIC 7106205. *MNRAS* 444, 1909–1918. doi:10.1093/mnras/stu1583, arXiv:1408.0715.
- Bradley, P.A., Guzik, J.A., Miles, L.F., Uytterhoeven, K., Jackiewicz, J., Kinemuchi, K., 2015. Results of a Search for γ Dor and δ Scuti Stars With the Kepler Spacecraft. *AJ* 149, 68. doi:10.1088/0004-6256/149/2/68, arXiv:1502.00928.
- Breger, M., 2000. δ Scuti stars (Review), in: Breger, M., Montgomery, M. (Eds.), *Delta Scuti and Related Stars*, p. 3.
- Breger, M., Fossati, L., Balona, L., Kurtz, D.W., Robertson, P., Bohlender, D., Lenz, P., Müller, I., Lüftinger, T., Clarke, B.D., Hall, J.R., Ibrahim, K.A., 2012. Relationship between Low and High Frequencies in δ Scuti Stars: Photometric Kepler and Spectroscopic Analyses of the Rapid Rotator KIC 8054146. *ApJ* 759, 62. doi:10.1088/0004-637X/759/1/62, arXiv:1209.4836.
- Breger, M., Handler, G., Garrido, R., Audard, N., Zima, W., Paparó, M., Beichbuchner, F., Li, Z.P., Jiang, S.Y., Liu, Z.L., Zhou, A.Y., Pikall, H., Schmalwieser, A., et al., 1999. 30+ frequencies for the delta Scuti variable 4 Canum Venaticorum: results of the 1996 multisite campaign. *A&A* 349, 225–235.
- Breger, M., Lenz, P., Antoci, V., Guggenberger, E., Shobbrook, R.R., Handler, G., Ngwato, B., Rodler, F., Rodriguez, E., López de Coca, P., Rolland, A., Costa, V., 2005. Detection of 75+ pulsation frequencies in the δ Scuti star FG Virginius. *A&A* 435, 955–965. doi:10.1051/0004-6361:20042480, arXiv:astro-ph/0502073.
- Breger, M., Montgomery, M.H., 2014. Evidence of Resonant Mode Coupling and the Relationship between Low and High Frequencies in a Rapidly Rotating a Star. *ApJ* 783, 89. doi:10.1088/0004-637X/783/2/89, arXiv:1402.0833.
- Breger, M., Stich, J., Garrido, R., Martin, B., Jiang, S.Y., Li, Z.P., Hube, D.P., Ostermann, W., Paparo, M., Scheck, M., 1993. Nonradial pulsation of the delta Scuti star BU CANCRI in the Praesepe cluster. *A&A* 271, 482–486.
- Chapellier, E., Mathias, P., 2013. The CoRoT star ID 100866999: a hybrid γ Doradus- δ Scuti star in an eclipsing binary system. *A&A* 556, A87. doi:10.1051/0004-6361/201321907, arXiv:1307.1268.
- Chen, X., Ding, X., Cheng, L., Zhang, X., Li, Y., Ji, K., Xiong, J., Li, X., Luo, C., 2022. Detection of δ Scuti Pulsators in the Eclipsing Binaries Observed by TESS. *ApJS* 263, 34. doi:10.3847/1538-4365/aca284.
- Chen, X., Wang, S., Deng, L., de Grijs, R., Yang, M., Tian, H., 2020. The Zwicky Transient Facility Catalog of Periodic Variable Stars. *ApJS* 249, 18. doi:10.3847/1538-4365/ab9cae, arXiv:2005.08662.
- Chen, X.H., Li, Y., Lai, X.J., Wu, T., 2016. Asteroseismology of the δ Scuti star HD 50844. *A&A* 593, A69. doi:10.1051/0004-6361/201628197, arXiv:1606.09324.
- Christy, C.T., Jayasinghe, T., Stanek, K.Z., Kochanek, C.S., Thompson, T.A., Shappee, B.J., Holoiien, T.W.S., Prieto, J.L., Dong, S., Giles, W., 2022. The ASAS-SN Catalog of Variable Stars X: Discovery of 116,000 New Variable Stars Using g-band Photometry. arXiv e-prints, arXiv:2205.02239arXiv:2205.02239.
- Cousins, A.W.J., Warren, P.R., 1963. Variable Stars Observed During the Cape Bright Star Programme. *Monthly Notes of the Astronomical Society of South Africa* 22, 65.
- Cunha, M.S., Antoci, V., Holdsworth, D.L., Kurtz, D.W., Balona, L.A., Bognár, Z., Bowman, D.M., Guo, Z., et al., 2019. Rotation and pulsation in Ap stars: first light results from TESS sectors 1 and 2. *MNRAS* 487, 3523–3549. doi:10.1093/mnras/stz1332, arXiv:1906.01111.
- Daszyńska-Daszkiewicz, J., Pamyatnykh, A.A., Walczak, P., Handler, G., Pigulski, A., Szewczuk, W., 2021. Mode identification and seismic study of δ Scuti, the prototype of a class of pulsating

- stars. *MNRAS* 505, 88–102. doi:10.1093/mnras/stab1292, arXiv:2105.00905.
- Demory, B.O., Pozuelos, F.J., Gómez Maqueo Chew, Y., Sabin, L., Petrucci, R., Schroffenegger, U., Grimm, S.L., Sestovic, M., et al., 2020. A super-Earth and a sub-Neptune orbiting the bright, quiet M3 dwarf TOI-1266. *A&A* 642, A49. doi:10.1051/0004-6361/202038616, arXiv:2009.04317.
- Du, B.T., Zhou, A.Y., Zhang, X.B., Liu, Z.L., Zhang, R.X., Li, H.B., Jinag, Z.J., Dong, X.Y., Zhao, L.M., 1999. A Newly Discovered Delta Scuti Variable Star. *Information Bulletin on Variable Stars* 4805, 1.
- Dumusque, X., Turner, O., Dorn, C., Eastman, J.D., Allart, R., Adibekyan, V., Sousa, S., Santos, N.C., Vanderspek, R.K., et al., 2019. Hot, rocky and warm, puffy super-Earths orbiting TOI-402 (HD 15337). *A&A* 627, A43. doi:10.1051/0004-6361/201935457, arXiv:1903.05419.
- Dupret, M.A., Grigahcène, A., Garrido, R., Gabriel, M., Scuflaire, R., 2005. Convection-pulsation coupling. II. Excitation and stabilization mechanisms in δ Sct and γ Dor stars. *A&A* 435, 927–939. doi:10.1051/0004-6361:20041817.
- Gaia Collaboration, Prusti, T., de Bruijne, J.H.J., Brown, A.G.A., Vallenari, A., Babusiaux, C., Bailer-Jones, C.A.L., Bastian, U., Peltzer, C., et al., 2016. The Gaia mission. *A&A* 595, A1. doi:10.1051/0004-6361/201629272, arXiv:1609.04153.
- Gaia Collaboration, Vallenari, A., et al., 2022. Gaia DR3: data release content and main properties. *A&A* 616, A1. doi:10.1051/0004-6361/201833051, arXiv:2206.09365.
- Ginsburg, A., Sipőcz, B.M., Brasseur, C.E., Cowperthwaite, P.S., Craig, M.W., Deil, C., et al., Astroquery Collaboration, 2019. astroquery: An Astronomical Web-querying Package in Python. *AJ* 157, 98. doi:10.3847/1538-3881/aaf333, arXiv:1901.04520.
- Gray, R.O., Corbally, Christopher, J., 2009. *Stellar Spectral Classification*.
- Grigahcène, A., Antoci, V., Balona, L., Catanzaro, G., Daszyńska-Daszkiewicz, J., Guzik, J.A., Handler, G., Houdek, G., et al., 2010. Hybrid γ Doradus- δ Scuti Pulsators: New Insights into the Physics of the Oscillations from Kepler Observations. *ApJL* 713, L192–L197. doi:10.1088/2041-8205/713/2/L192, arXiv:1001.0747.
- Guzik, J.A., Jackiewicz, J., Hedlund, A.M., 2022. Revisiting the δ Scuti star FG Virginis using Kepler K2 and TESS data. *Frontiers in Astronomy and Space Sciences* 9, 948180. doi:10.3389/fspas.2022.948180.
- Guzik, J.A., Kaye, A.B., Bradley, P.A., Cox, A.N., Neuforge, C., 2000. Driving the Gravity-Mode Pulsations in γ Doradus Variables. *ApJL* 542, L57–L60. doi:10.1086/312908.
- Handberg, R., Lund, M.N., White, T.R., Hall, O.J., Buzasi, D.L., Pope, B.J.S., Tenenbaum, P., et al., T'DA Collaboration, 2021. TESS Data for Asteroseismology: Photometry. *AJ* 162, 170. doi:10.3847/1538-3881/ac09f1, arXiv:2106.08341.
- Handler, G., 1999. The domain of γ Doradus variables in the Hertzsprung-Russell diagram. *MNRAS* 309, L19–L23. doi:10.1046/j.1365-8711.1999.03005.x.
- Handler, G., 2009a. Confirmation of simultaneous p and g mode excitation in HD 8801 and γ Peg from time-resolved multi-colour photometry of six candidate ‘hybrid’ pulsators. *MNRAS* 398, 1339–1351. doi:10.1111/j.1365-2966.2009.15005.x, arXiv:0904.4859.
- Handler, G., 2009b. Delta Scuti Variables, in: Guzik, J.A., Bradley, P.A. (Eds.), *Stellar Pulsation: Challenges for Theory and Observation*, pp. 403–409. doi:10.1063/1.3246528, arXiv:2110.09806.
- Handler, G., 2009c. “Hybrid” pulsators - fact or fiction? *Communications in Asteroseismology* 159, 42–44. doi:10.1553/cia159s42.
- Handler, G., 2012. Hybrid Pulsators among A/F-type Stars, in: Shibahashi, H., Takata, M., Lynas-Gray, A.E. (Eds.), *Progress in Solar/Stellar Physics with Helio- and Asteroseismology*, p. 111. arXiv:1112.5981.
- Hareter, M., Fossati, L., Weiss, W., Suárez, J.C., Uytterhoeven, K., Rainer, M., Poretti, E., 2011. Looking for a Connection between the Am Phenomenon and Hybrid δ Sct- γ Dor Pulsation: Determination of the Fundamental Parameters and Abundances of HD 114839 and BD +18 4914. *ApJ* 743, 153. doi:10.1088/0004-637X/743/2/153, arXiv:1109.2742.
- Harris, C.R., Millman, K.J., van der Walt, S.J., Gommers, R., Virtanen, P., Cournapeau, D., Gohlke, C., et al., 2020. Array programming with NumPy. *Nature* 585, 357–362. URL: <https://doi.org/10.1038/s41586-020-2649-2>, doi:10.1038/s41586-020-2649-2.
- Henry, G.W., Fekel, F.C., 2005. HD 8801: A Unique Single Am Star with γ Doradus and δ Scuti Pulsations. *AJ* 129, 2026–2033. doi:10.1086/428373.
- Henry, G.W., Fekel, F.C., Henry, S.M., 2005. Eleven New γ Doradus Stars. *AJ* 129, 2815–2830. doi:10.1086/429876.
- Henry, G.W., Fekel, F.C., Henry, S.M., 2007. Photometry and Spectroscopy of 11 γ Doradus Stars. *AJ* 133, 1421–1440. doi:10.1086/511820.
- Henry, G.W., Fekel, F.C., Henry, S.M., 2011. A Volume-limited Photometric Survey of 114 γ Doradus Candidates. *AJ* 142, 39. doi:10.1088/0004-6256/142/2/39, arXiv:1105.4161.
- Henry, G.W., Fekel, F.C., Williamson, M.H., 2022. Nine Bright γ Doradus Variables Discovered with Ground-based Photometry. *AJ* 163, 180. doi:10.3847/1538-3881/ac540b.
- Hill, K.L., Littlefield, C., Garnavich, P., Scaringi, S., Szkody, P., Mason, P.A., Kennedy, M.R., Shaw, A.W., Covington, A.E., 2022. Hitting a New Low: The Unique 28 hr Cessation of Accretion in the TESS Light Curve of YY Dra (DO Dra). *AJ* 163, 246. doi:10.3847/1538-3881/ac5a51, arXiv:2203.00221.
- Hon, M., Huber, D., Kuszlewicz, J.S., Stello, D., Sharma, S., Tayar, J., Zinn, J.C., Vrad, M., Pinsonneault, M.H., 2021. A “Quick Look” at All-sky Galactic Archeology with TESS: 158,000 Oscillating Red Giants from the MIT Quick-look Pipeline. *ApJ* 919, 131. doi:10.3847/1538-4357/ac14b1, arXiv:2108.01241.
- Huber, D., White, T.R., Metcalfe, T.S., Chontos, A., Fausnaugh, M.M., Ho, C.S.K., et al., 2022. A 20 Second Cadence View of Solar-type Stars and Their Planets with TESS: Asteroseismology of Solar Analogs and a Recharacterization of π Men c. *AJ* 163, 79. doi:10.3847/1538-3881/ac3000, arXiv:2108.09109.
- Hunter, J.D., 2007. Matplotlib: A 2d graphics environment. *Computing in Science & Engineering* 9, 90–95. doi:10.1109/MCSE.2007.55.
- Ivezić, Ž., Kahn, S.M., Tyson, J.A., Abel, B., Acosta, E., Allsmann, R., Alonso, D., AlSayyad, Y., Anderson, S.F., Andrew, J., Angel, J.R.P., Angeli, G.Z., Ansari, R., Antilogus, P., Araujo, C., Armstrong, R., Arndt, K.T., Astier, P., et al., 2019. LSST: From Science Drivers to Reference Design and Anticipated Data Products. *ApJ* 873, 111. doi:10.3847/1538-4357/ab042c, arXiv:0805.2366.
- Jeffery, C.S., 2008. The impact of asteroseismology on the theory of stellar evolution. *Communications in Asteroseismology* 157, 240–248.
- Jurcsik, J., Sódor, Á., Hajdu, G., Szeidl, B., Dózsa, Á., Posztobányi, K., Smitola, P., Belucz, B., Fehér, V., Kővári, Z., Kriskovics, L., Kun, E., Molnár, L., Nagy, I., Vida, K., Görög, N., 2012. An extensive photometric study of the Blazhko RR Lyrae star RZ Lyr. *MNRAS* 423, 993–1005. doi:10.1111/j.1365-2966.2012.20772.x, arXiv:1202.4388.
- Kallinger, T., Reegen, P., Weiss, W.W., 2008. A heuristic derivation of the uncertainty for frequency determination in time series

- data. *A&A* 481, 571–574. doi:10.1051/0004-6361/20077559, arXiv:0801.0683.
- Kallinger, T., Weiss, W.W., Beck, P.G., Pigulski, A., Kuschnig, R., Tkachenko, A., Wade, G.A., et al., 2017. Triple system HD 201433 with a SPB star component seen by BRITE - Constellation: Pulsation, differential rotation, and angular momentum transfer. *A&A* 603, A13. doi:10.1051/0004-6361/201730625, arXiv:1704.01151.
- Kaye, A.B., Handler, G., Krisciunas, K., Poretti, E., Zerbi, F.M., 1999. Gamma Doradus Stars: Defining a New Class of Pulsating Variables. *PASP* 111, 840–844. doi:10.1086/316399, arXiv:astro-ph/9905042.
- Kazarovets, E.V., Samus, N.N., Durevich, O.V., 2022. Revised Version of the New Catalogue of Suspected Variable Stars, NSV Release 2. *Astronomy Reports* 66, 555–560. doi:10.1134/S1063772922080066.
- Kirmizitas, O., Cavus, S., Kahraman Aliçavuş, F., 2022. Discovery of new Delta Scuti Stars. arXiv e-prints, arXiv:2208.11915arXiv:2208.11915.
- Koen, C., van Wyk, F., Laney, C.D., Kilkeny, D., 2017. HR 7920: a very bright new Delta Scuti star with possible Gamma Doradus variations. *MNRAS* 466, 122–128. doi:10.1093/mnras/stw3062.
- Krisciunas, K., 1993. A new class of pulsating stars, in: American Astronomical Society Meeting Abstracts, p. 84.02.
- Krisciunas, K., 1998. The discovery of non-radial gravity-mode pulsations in gamma Doradus-type stars, in: Deubner, F.L., Christensen-Dalsgaard, J., Kurtz, D. (Eds.), *New Eyes to See Inside the Sun and Stars*, p. 339. arXiv:astro-ph/9707249.
- Krisciunas, K., Handler, G., 1995. A List of Variable Stars Similar to gamma Dor. *Information Bulletin on Variable Stars* 4195, 1.
- Kurtz, D.W., 1979. The frequency analysis of low-amplitude delta Scuti stars - II. HD 52788: a new variable delta Delphini star. *MNRAS* 186, 575–582. doi:10.1093/mnras/186.3.575.
- Kurtz, D.W., 1981. The frequency analysis of low amplitude del SCT stars. - VI. Further observations of HD 52788. *MNRAS* 194, 39–47. doi:10.1093/mnras/194.1.39.
- Lenz, P., Breger, M., 2005. *Period04 User Guide*. *Communications in Asteroseismology* 146, 53–136. doi:10.1553/cia146s53.
- Li, G., Guo, Z., Fuller, J., Bedding, T.R., Murphy, S.J., Colman, I.L., Hey, D.R., 2020a. The effect of tides on near-core rotation: analysis of 35 Kepler γ Doradus stars in eclipsing and spectroscopic binaries. *MNRAS* 497, 4363–4375. doi:10.1093/mnras/staa2266, arXiv:2007.14853.
- Li, G., Van Reeth, T., Bedding, T.R., Murphy, S.J., Antoci, V., Ouazani, R.M., Barbara, N.H., 2020b. Gravity-mode period spacings and near-core rotation rates of 611 γ Doradus stars with Kepler. *MNRAS* 491, 3586–3605. doi:10.1093/mnras/stz2906, arXiv:1910.06634.
- Littlefield, C., Scaringi, S., Garnavich, P., Szkody, P., Kennedy, M.R., Ikwicz, K., Mason, P.A., 2021. Quasi-periodic Oscillations in the TESS Light Curve of TX Col, a Diskless Intermediate Polar on the Precipice of Forming an Accretion Disk. *AJ* 162, 49. doi:10.3847/1538-3881/ac062b, arXiv:2104.14140.
- Loumos, G.L., Deeming, T.J., 1978. Spurious Results from Fourier Analysis of Data with Closely Spaced Frequencies. *Ap&SS* 56, 285–291. doi:10.1007/BF01879560.
- Lund, M.N., Handberg, R., Buzasi, D.L., Carboneau, L., Hall, O.J., Pereira, F., Huber, D., Hey, D., Van Reeth, T., T'DA Collaboration, 2021. TESS Data for Asteroseismology: Light-curve Systematics Correction. *ApJS* 257, 53. doi:10.3847/1538-4365/ac214a, arXiv:2108.11780.
- Ma, S., Esamdin, A., Hernández, A.G., Murphy, S.J., Lv, C., Wei, P., Rieutord, M., Pascual-Granado, J., Dang, F., Niu, H., Yang, T., Feng, G., Karimov, R., Tillayev, Y., 2022. KIC 3440495: A Rapidly Rotating δ Scuti- γ Doradus Hybrid Pulsator in a Binary System. *ApJ* 937, 80. doi:10.3847/1538-4357/ac8c30.
- Maschi, F.J., Laher, R.R., Rusholme, B., Shupe, D.L., Groom, S., Surace, J., Jackson, E., Monkewitz, S., Beck, R., Flynn, D., et al., 2019. The Zwicky Transient Facility: Data Processing, Products, and Archive. *PASP* 131, 018003. doi:10.1088/1538-3873/aae8ac, arXiv:1902.01872.
- Montgomery, M.H., O'Donoghue, D., 1999. A derivation of the errors for least squares fitting to time series data. *Delta Scuti Star Newsletter* 13, 28.
- Murphy, S.J., 2012. An examination of some characteristics of Kepler short- and long-cadence data. *MNRAS* 422, 665–671. doi:10.1111/j.1365-2966.2012.20644.x, arXiv:1201.6184.
- Murphy, S.J., Hey, D., Van Reeth, T., Bedding, T.R., 2019. Gaia-derived luminosities of Kepler A/F stars and the pulsator fraction across the δ Scuti instability strip. *MNRAS* 485, 2380–2400. doi:10.1093/mnras/stz590, arXiv:1903.00015.
- Ofek, E.O., Soumagnac, M., Nir, G., Gal-Yam, A., Nugent, P., Maschi, F., Kulkarni, S.R., 2020. A catalogue of over 10 million variable source candidates in ZTF Data Release 1. *MNRAS* 499, 5782–5790. doi:10.1093/mnras/staa2814, arXiv:2007.01537.
- Oliveira da Rosa, G., Kepler, S.O., Córscico, A.H., Costa, J.E.S., Hermes, J.J., Kawaler, S.D., Clemens, J.C., et al., 2022. Kepler and TESS Observations of PG 1159-035. *ApJ* 936, 187. doi:10.3847/1538-4357/ac8871, arXiv:2208.04791.
- Paegert, M., Stassun, K.G., Collins, K.A., Pepper, J., Torres, G., Jenkins, J., Twicken, J.D., Latham, D.W., 2021. TESS Input Catalog versions 8.1 and 8.2: Phantoms in the 8.0 Catalog and How to Handle Them. arXiv e-prints, arXiv:2108.04778arXiv:2108.04778.
- Paunzen, E., Bernhard, K., Hümmerich, S., Hambusch, F.J., Lloyd, C., Otero, S., 2020. High-amplitude γ Doradus variables. *MNRAS* 499, 3976–3991. doi:10.1093/mnras/staa2905, arXiv:2009.09239.
- Pietrukowicz, P., Soszyński, I., Netzel, H., Wrona, M., Udalski, A., Szymański, M.K., et al., 2020. Over 10000 δ Scuti Stars toward the Galactic Bulge from OGLE-IV. *Acta Astronomica* 70, 241–263. doi:10.32023/0001-5237/70.4.1, arXiv:2103.10436.
- Pollard, K.R., 2009. A Review Of γ Doradus Variables, in: Guzik, J.A., Bradley, P.A. (Eds.), *Stellar Pulsation: Challenges for Theory and Observation*, pp. 455–466. doi:10.1063/1.3246543.
- Poretti, E., Michel, E., Garrido, R., Lefèvre, L., Mantegazza, L., Rainer, M., Rodríguez, E., Uytterhoeven, K., Pápics, P., et al., 2009. HD 50844: a new look at δ Scuti stars from CoRoT space photometry. *A&A* 506, 85–93. doi:10.1051/0004-6361/200912039.
- Prša, A., Kochoska, A., Conroy, K.E., Eisner, N., Hey, D.R., Ijspeert, L., et al., 2022. TESS Eclipsing Binary Stars. I. Short-cadence Observations of 4584 Eclipsing Binaries in Sectors 1–26. *ApJS* 258, 16. doi:10.3847/1538-4365/ac324a, arXiv:2110.13382.
- Qian, S.B., Li, L.J., He, J.J., Zhang, J., Zhu, L.Y., Han, Z.T., 2018. LAMOST views δ Scuti pulsating stars. *MNRAS* 475, 478–491. doi:10.1093/mnras/stx3185, arXiv:1707.04006.
- Ricker, G.R., Winn, J.N., Vanderspek, R., Latham, D.W., Bakos, G.Á., Bean, J.L., Berta-Thompson, Z.K., Brown, T.M., Buchhave, L., Butler, N.R., Butler, R.P., Chaplin, W.J., Charbonneau, D., et al., 2015. Transiting Exoplanet Survey Satellite (TESS). *Journal of Astronomical Telescopes, Instruments, and Systems* 1, 014003. doi:10.1117/1.JATIS.1.1.014003.
- Rodríguez, E., 2023. Private communication. E-mail, IAA-CSIC, Spain.
- Rodríguez, E., Breger, M., 2001. delta Scuti and related stars: Analysis of the R00 Catalogue. *A&A* 366, 178–196. doi:10.1051/0004-6361/20000205.
- Rowe, J.F., Matthews, J.M., Cameron, C., Bohlender, D.A., King, H., Kuschnig, R., Guenther, D.B., Moffat, A.F.J., Rucinski, S.M., Sas-

- selov, D., Walker, G.A.H., Weiss, W.W., 2006. Discovery of hybrid γ Dor and δ Sct pulsations in BD+18 4914 through MOST space-based photometry. *Communications in Asteroseismology* 148, 34–43. doi:10.1553/cia148s34, arXiv:astro-ph/0610640.
- Samus, N.N., Kazarovets, E.V., Durevich, O.V., Kireeva, N.N., Pastukhova, E.N., 2017. General catalogue of variable stars: Version GCVS 5.1. *Astronomy Reports* 61, 80–88. doi:10.1134/S1063772917010085.
- Shi, X.d., Qian, S.b., Li, L.j., Liao, W.p., 2021a. HL Dra: an active Algol-like binary system with a pulsating component star and a cool third body. *MNRAS* 505, 6166–6178. doi:10.1093/mnras/stab1657.
- Shi, X.d., Qian, S.b., Li, L.j., Zhao, E.g., 2021b. CSS J213934.3-050020: A New Double-mode High-amplitude δ Scuti-type Pulsating Star. *PASP* 133, 054201. doi:10.1088/1538-3873/abf32a.
- Shporer, A., Wong, I., Huang, C.X., Line, M.R., Stassun, K.G., Fetherolf, T., Kane, S.R., Bouma, L.G., Daylan, T., Günther, M.N., Ricker, G.R., Latham, D.W., Vanderspek, R., Seager, S., Winn, J.N., Jenkins, J.M., Glidden, A., Berta-Thompson, Z., Ting, E.B., Li, J., Haworth, K., 2019. TESS Full Orbital Phase Curve of the WASP-18b System. *AJ* 157, 178. doi:10.3847/1538-3881/ab0f96, arXiv:1811.06020.
- Soszyński, I., Pietrukowicz, P., Skowron, J., Udalski, A., Szymański, M.K., Skowron, D.M., Poleski, R., Kozłowski, S., Mróz, P., Ulaczyk, K., Rybicki, K., Iwanek, P., Wrona, M., Gromadzki, M., 2021. Over 24 000 δ Scuti Stars in the Galactic Bulge and Disk from the OGLE Survey. *Acta Astronomica* 71, 189–204. doi:10.32023/0001-5237/71.3.1, arXiv:2111.03072.
- Southworth, J., Van Reeth, T., 2022a. Four bright eclipsing binaries with γ Doradus pulsating components: CM Lac, MZ Lac, RX Dra, and V2077 Cyg. *MNRAS* 515, 2755–2765. doi:10.1093/mnras/stac1993, arXiv:2207.09169.
- Southworth, J., Van Reeth, T., 2022b. Four bright eclipsing binaries with gamma Doradus pulsating components: CM Lac, MZ Lac, RX Dra and V2077 Cyg. arXiv e-prints , arXiv:2207.09169arXiv:2207.09169.
- Southworth, J., Zima, W., Aerts, C., Bruntt, H., Lehmann, H., Kim, S.L., Kurtz, D.W., Pavlovski, K., Prša, A., Smalley, B., Gilliland, R.L., Christensen-Dalsgaard, J., Kawaler, S.D., Kjeldsen, H., Cote, M.T., Tenenbaum, P., Twicken, J.D., 2011. Kepler photometry of KIC 10661783: a binary star with total eclipses and δ Scuti pulsations. *MNRAS* 414, 2413–2423. doi:10.1111/j.1365-2966.2011.18559.x, arXiv:1102.3599.
- Stassun, K.G., Oelkers, R.J., Paegert, M., Torres, G., Pepper, J., De Lee, N., Collins, K., Latham, D.W., et al., 2019. The Revised TESS Input Catalog and Candidate Target List. *AJ* 158, 138. doi:10.3847/1538-3881/ab3467, arXiv:1905.10694.
- Stassun, K.G., Oelkers, R.J., Pepper, J., Paegert, M., De Lee, N., Torres, G., Latham, D.W., Charpinet, S., Dressing, C.D., Huber, D., Kane, S.R., Lépine, S., Mann, A., Muirhead, P.S., Rojas-Ayala, B., Silvotti, R., Fleming, S.W., Levine, A., Plavchan, P., 2018. The TESS Input Catalog and Candidate Target List. *AJ* 156, 102. doi:10.3847/1538-3881/aad050, arXiv:1706.00495.
- Steindl, T., Zwintz, K., Bowman, D.M., 2021. Tidally perturbed pulsations in the pre-main sequence δ Scuti binary RS Cha. *A&A* 645, A119. doi:10.1051/0004-6361/202039093, arXiv:2011.08214.
- Szabados, L., 2014. Pulsating stars — plethora of variables and observational tasks. *Contributions of the Astronomical Observatory Skalnaté Pleso* 43, 338–350.
- Telting, J.H., Østensen, R.H., Baran, A.S., Bloemen, S., Reed, M.D., Oreiro, R., Farris, L., Ottosen, T.A., Aerts, C., Kawaler, S.D., Heber, U., Prins, S., Green, E.M., Kalomeni, B., O’Toole, S.J., Mullally, F., Sanderfer, D.T., Smith, J.C., Kjeldsen, H., 2012. Three ways to solve the orbit of KIC 11 558 725: a 10-day beam-
ing sdB+WD binary with a pulsating subdwarf. *A&A* 544, A1. doi:10.1051/0004-6361/201219458, arXiv:1206.3872.
- The Astropy Collaboration, Price-Whelan, A.M., Sipőcz, B.M., Günther, H.M., Lim, P.L., Crawford, S.M., Conseil, S., Shupe, D.L., Craig, M.W., Dencheva, N., Ginsburg, A., VanderPlas, J.T., Woillez, J., et al., Contributors, ., 2018a. The Astropy Project: Building an Open-science Project and Status of the v2.0 Core Package. *AJ* 156, 123. doi:10.3847/1538-3881/aabc4f, arXiv:1801.02634.
- The Astropy Collaboration, Price-Whelan, A.M., Sipőcz, B.M., Günther, H.M., Lim, P.L., Crawford, S.M., Conseil, S., Shupe, D.L., Craig, M.W., Dencheva, N., Ginsburg, A., VanderPlas, J.T., Woillez, J., et al., Contributors, ., 2018b. The Astropy Project: Building an Open-science Project and Status of the v2.0 Core Package. *AJ* 156, 123. doi:10.3847/1538-3881/aabc4f, arXiv:1801.02634.
- Virtanen, P., Gommers, R., Oliphant, T.E., Haberland, M., Reddy, T., Cournapeau, D., Burovski, E., Peterson, P., Pedregosa, F., et al., SciPy 1.0 Contributors, 2020. SciPy 1.0: Fundamental Algorithms for Scientific Computing in Python. *Nature Methods* 17, 261–272. doi:10.1038/s41592-019-0686-2.
- von Essen, C., Mallonn, M., Borre, C.C., Antoci, V., Stassun, K.G., Khalafinejad, S., Tautvaišienė, G., 2020. TESS unveils the phase curve of WASP-33b. Characterization of the planetary atmosphere and the pulsations from the star. *A&A* 639, A34. doi:10.1051/0004-6361/202037905, arXiv:2004.10767.
- Watson, C., Henden, A.A., Price, A., 2022. VizieR Online Data Catalog: AAVSO International Variable Star Index VSX (Watson+, 2006-2014). VizieR Online Data Catalog , B/vsx.
- Watson, C.L., Henden, A.A., Price, A., 2006. The International Variable Star Index (VSX). *Society for Astronomical Sciences Annual Symposium* 25, 47.
- Xiong, D.R., Deng, L., Zhang, C., Wang, K., 2016. Turbulent convection and pulsation stability of stars - II. Theoretical instability strip for δ Scuti and γ Doradus stars. *MNRAS* 457, 3163–3177. doi:10.1093/mnras/stw047, arXiv:1808.09621.
- Zhang, X., Chen, X., Zhang, H., Fu, J., Li, Y., 2020. A Pre-main-sequence γ Dor- δ Sct Hybrid with Extremely Slow Internal Rotation in a Short-period Eclipsing Binary KIC 9850387 Revealed by Asteroseismology. *ApJ* 895, 124. doi:10.3847/1538-4357/ab8ad5.
- Zhang, X.B., Deng, L.C., Luo, C.Q., 2012. A Probable Hybrid γ Dor- δ Scuti Variable Discovered in the Open Cluster NGC 2126. *AJ* 144, 141. doi:10.1088/0004-6256/144/5/141.
- Zhang, X.B., Wang, K., Chen, X.H., Luo, C.Q., Zhang, C.G., 2019. Discovery and Seismic Analysis of an EL CVn-type Binary with Hybrid δ Sct- γ Dor Pulsations. *ApJ* 884, 165. doi:10.3847/1538-4357/ab3fa9.
- Zhou, A.Y., 2004. Time-dependent Behaviour of the Low Amplitude δ Scuti Star HD 52788. *ChJAA (Chin. J. Astron. Astrophys.)* 4, 335–342. doi:10.1088/1009-9271/4/4/335.
- Zhou, A.Y., 2015. Hybrid Pulsators – Pulsating Stars with Multiple Identities. arXiv e-prints , arXiv:1501.05166arXiv:1501.05166.
- Zhou, A.Y., An, D., Eggen, J.R., Reed, M.D., Terndrup, D.M., Harms, S.L., 2006. Discovery of a New Multiperiodic δ Scuti Variable Star. *Ap&SS* 305, 29–36. doi:10.1007/s10509-005-9034-3.